MICROCOPY RESOLUTION TEST CHART

NATIONAL BUREAU OF STANDARDS-1963-A

AFGL-TR-77-0022

STATIC AND DYNAMIC CALIBRATION
OF A CORONA DISCHARGE ANEMOMETER

Frank H. Durgin
Jerome P. Fanucci

Massachusetts Institute of Technology
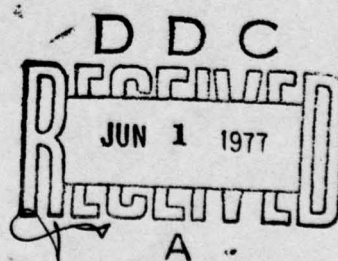77 Massachusetts Avenue
Cambridge, Massachusetts   02139

Final Report
April 1976 to December 1976

December 1976

Approved for public release; distribution unlimited

DDC
RECEIVED
JUN 1 1977
A

REPORT DOCUMENTATION PAGE	READ INSTRUCTIONS BEFORE COMPLETING FORM
1. REPORT NUMBER (19) AFGL-TR-77-0022	2. GOVT ACCESSION NO	3. RECIPIENT'S CATALOG NUMBER

4. TITLE (and Subtitle) Static and Dynamic Calibration of a Corona Discharge Anemometer.	5. TYPE OF REPORT & PERIOD COVERED Final rept. Apr 1976-Dec 1976
	6. PERFORMING ORG. REPORT NUMBER WBWT-TR-1101
7. AUTHOR(s) Frank H. Durgin Jerome P. Fanucci	8. CONTRACT OR GRANT NUMBER(s) F19628-76-C-0145 new
9. PERFORMING ORGANIZATION NAME AND ADDRESS Massachusetts Institute of Technology 77 Massachusetts Ave. Cambridge, MA 02139	10. PROGRAM ELEMENT, PROJECT, TASK AREA & WORK UNIT NUMBERS 62101F 668705 05
11. CONTROLLING OFFICE NAME AND ADDRESS Air Force Geophysics Laboratory (LKC) Hanscom AFB, Massachusetts 01731 Monitor/James H. Brown/LKC	12. REPORT DATE Dec 1976
	13. NUMBER OF PAGES 71 72 p.
14. MONITORING AGENCY NAME & ADDRESS(if different from Controlling Office)	15. SECURITY CLASS. (of this report) Unclassified
	15a. DECLASSIFICATION DOWNGRADING SCHEDULE

16. DISTRIBUTION STATEMENT (of this Report)

Approved for public release; distribution unlimited

17. DISTRIBUTION STATEMENT (of the abstract entered in Block 20, if different from Report)

18. SUPPLEMENTARY NOTES

19. KEY WORDS (Continue on reverse side if necessary and identify by block number)

Anemometer   Frequency Response
Corona Discharge
Static Calibration
Dynamic Calibration

20. ABSTRACT (Continue on reverse side if necessary and identify by block number)

A Corona Discharge Anemometer (CDA) which is to be used in some balloon experiments designed to measure clear air turbulence, has been tested in the Wright Brothers Wind Tunnel at the Massachusetts Institute of Technology. First a modified version of the anemometer commercially made by Thermo Systems Inc. was tested statically to determine its sensitivity, its ability to resolve the x and y components of velocity and the effect of out of plane flow on its sensitivity.

DD FORM 1473 EDITION OF 1 NOV 65 IS OBSOLETE
1 JAN 73

381 750

FOREWORD

iii

ABSTRACT

A Corona Discharge Anemometer (CDA) which is to be used in some balloon experiments designed to measure clear air turbulence, has been tested in the Wright Brothers Wind Tunnel at the Massachusetts Institute of Technology. First a modified version of the anemometer commercially made by Thermo Systems Inc. was tested statically to determine its sensitivity, its ability to resolve the x and y components of velocity and the effect of out of plane flow on its sensitivity.

The CDA performed adequately except that there was a periodic change in sensitivity with the in-plane angle of flow due to the 16 posts used to create the gap between the two parts of the cylinder in which the velocity is measured.

The CDA was then used to measure the turbulence in a known flow to determine its ability to measure turbulence. These tests showed that there was both electrical and aerodynamic noise generated by the device. No attempt was made to determine the sources of the electrical noise, but the aerodynamic noise was found to be from two sources; vortex shedding from the posts, and a flow separation at the entrance of the measuring channel.

A model of the CDA to be used in an actual test was then tested. Increasing the gap between the 3" cylinders from 1/2" to 1" and the entrance radius from 1/32" to 1/16" did not reduce the noise from the entrance separation. However, increasing the entrance radius to 1/2" essentially eliminated the entrance separation and any noise from it.

iv

TABLE OF CONTENTS

LIST OF ILLUSTRATIONS

LIST OF ILLUSTRATIONS (Continued)

LIST OF ILLUSTRATIONS (Concluded)

LIST OF TABLES

SECTION 1

INTRODUCTION

At the request of the Air Force Geophysics Research Laboratory (AFGL), the Wright Brothers Wind Tunnel of the Department of Aeronautics and Astronautics of the Massachusetts Institute of Technology has undertaken to investigate the characteristics of a Corona Discharge Anemometer in turbulence. It is planned to use the anemometer to make measurements of clear air turbulence (CAT) from an instrumented balloon. It is believed that CAT is caused by instabilities in the boundary between a jet stream and the surrounding air. Since flows in this region are highly complex, it was deemed important to determine the response of the Corona Discharge Anemometer in flows with varying amounts of turbulence; to this end a five-part program was undertaken.

The first three phases of testing were designed to calibrate a Corona Discharge Anemometer (CDA) in steady and turbulent flow. The CDA was manufactured by Thermo Systems Inc. (TSI) and was modified by AFGL. Phase one consisted of measuring the properties of the flow in the empty wind tunnel for various combinations of free stream velocity and distance downstream from a turbulence generating grid. During phase two the TSI anemometer was calibrated statically in these known flows, and its sensitivity to velocity as a function of azimuth and pitch angle was studied. In phase three the anemometer's ability to measure turbulence intensity and frequency spectra was investigated.

The results from tests of the TSI instrument in phases 2 and 3 indicated that the anemometer's geometry caused problems that were inhibiting its ability to measure the free stream conditions accurately. Part four of the program was designed to define these problems better by using a hot wire to survey the velocity field inside of a full-scale model of the anemometer. This first model differed from the TSI instrument in that the gap between the ends of the two 3 inch diameter cylinders which formed the test section of the device had been increased from 1/2 to one inch to simulate better the anemometer actually used by AFGL for their CAT measurements. These tests confirmed the conjecture that leading edge separation was modifying the flow in the test section and therefore was affecting the velocity measured by the Corona Discharge device.

A second model was then built with the leading edge radius increased from 1/16" to 1/2" to attempt to reduce leading edge separation. Part five

1

of this program was conducted in essentially the same manner as part four, and showed that this modification did substantially reduce the separation of the flow.

2

SECTION 2

EQUIPMENT

2.1 The Wind Tunnel

The Wright Brothers Wind Tunnel is a closed return facility with a 10-ft. wide, 7.5 ft. high elliptical test section 15 ft. long (Fig. 1). A 2000-HP motor provides wind speeds up to 140 mph at atmospheric pressure. A separate fan can be installed to produce low turbulence flows at speeds up to 10 ft/sec. Turbulent flows were generated by installing a wooden grid at the beginning of the test section. The grid, constructed of a square lattice of 1" x 3" boards spaced 12" apart (Fig. 2) was designed using data from Baines & Peterson [1] to produce a flow which varied from 20% turbulence 2.5 ft. back from the grid to 5% at 15 ft.

2.2 The Models

2.2.1 The Corona Discharge Anemometer

The calibration runs, defined in the contract, were conducted on the modified TSI Corona Discharge Anemometer supplied by AFCL. The anemometer measures the free stream flow by sensing the wind induced changes of the flow of charged particles across a gap between two flat plates. Physically this instrument resembled two solid 3" diameter cylinders separated by a constant 1/2" gap between their ends. This gap, which was maintained by sixteen 1/16" dia. rods evenly spaced around the edge of the cylinders, was half the gap of the anemometer that was expected to be used by AFGL in their CAT experiments. The edges of the cylinders were finished with a very small radius (about 1/32"; Fig. 3).

The anemometer was mounted vertically on a stand supplied by AFGL. This stand was designed to permit variation of the static pitch angle in the XZ plane, as well as both static and dynamic changes of azimuth angle. Azimuth was varied dynamically by an electric motor on the stand that could impart spin rates of up to 0.55 rad/sec about the anemometer's vertical axis. It should be noted that this rate of change of azimuth was not sufficient for detection of any lag in indicated inflow angle caused by rapid changes in free stream direction.

3

2.2.2 Full Scale Corona Discharge Model

A full-scale aluminum model of the Corona Discharge Anemometer used in
the actual CAT measurements was built to study the effects of the changes in
the device's geometry on the flow in the test channel between the two cylinders
(Fig. 4). Since the model was intended only for aerodynamic investigations
of the flow in the channel, no internal electronics were included. This model
differed in two respects from the device previously tested: the gap between
the two cylinders was increased 1/2 to 1", and the edge radius was increased
from 1/32" to about 1/16" in an attempt to reduce flow separation at the leading
edge. This model was rigidly mounted to a heavy metal stand which placed the
test channel of the device 25 inches from the wind tunnel floor.

2.2.3 Modified Full Scale Corona Discharge Model

Smoke studies and internal velocity field measurements of the model as
discussed in Subsection 2.2.2 suggested that flow separation at the entrance
to the test section could be reduced by increasing the 1/16" edge radius of
the cylinders that formed the upper and lower surfaces of the test section
channel. A second full-scale model with a much larger entrance radius (1/2")
was constructed of solid plastic to investigate the effect of this modification
(Fig. 5). Note that the larger leading edge radius has increased the length
of the 16 supporting posts. This model was mounted on the same rigid support
as was the first model.

2.3 Instrumentation

A pitot-static probe was mounted in the plane of the Corona Discharge
Anemometer at the height of its test channel but displaced to one side in
order to be out of the flow field of the anemometer. The pressure head
measured by this probe was read on a Flow Corporation Model MM2 micromanometer
which enabled readings to be repeated to within a few ten thousandths of an
inch of alcohol, with corresponding accuracy in the free stream velocity
measurement ($\pm$ 15% at .3 m/sec. to $\pm$ .1% at 12 m/sec.).

Measurement of the fluctuating velocity was made using a Flow Corporation
Series 900 hot wire anemometer operated in the constant temperature mode and
linearized with a Flow Corporation 900-4 linearizer. With a platinum wire
0.1 inch long and 0.0005 inch in diameter, the entire system had an upper

4

frequency limit of about 1000 Hz. The fluctuating velocity component was measured directly from the linearizer output using a Hewlett-Packard (HP) model 3400A RMS voltmeter which had been modified to have a 20 second averaging time. This 20 second averaging time made the meter accurate to within 10% down to 2 Hz.

For measurement of the average velocity, the linearized signal was put through a two to one voltage divider composed of two 1% 5100 ohm resistors in series, with a 3000 MFD capacitor in parallel with the second resistor. The voltage across this lower RC pair, which corresponded to 1/2 the average velocity, was then read using an HP model 412A DC voltmeter. The 15 second time constant of the RC combination was chosen to reduce the time variations of the meter reading.

Velocity and direction data from the TSI were plotted using a 6-channel chart recorder supplied by AFGL for the tests. Some data from the hot wire was recorded on an HP 3960 FM tape recorder for frequency spectra analysis. A Federal Scientific Corporation Ubiquitous Spectrum Analyzer Model UA-14, together with a Spectrum Averager Model 1014, were used for all frequency spectra measurements.

SECTION 3

TESTING

The wind tunnel test program for the Corona Discharge Anemometer was divided into five phases:

3.1   Phase 1:   Wind Tunnel Calibration

To determine the conditions that would exist in the tunnel during the calibration of the Corona Discharge Anemometer, a series of measurements were made to define the characteristics of the flows generated by both the low turbulence fan and the main propeller, with and without the turbulence-generating grid installed, and with the Corona Discharge Anemometer removed from the test section. Free stream velocity was measured with the pitot static probe and a micromanometer, while the hot wire anemometer and associated electronics described in the previous section were used to measure the fluctuating component of velocity as well as frequency spectrum for various combinations of velocity and distance downstream from the turbulence generating grid. Besides allowing later tests to be conducted at known conditions, the tunnel calibration phase served to verify that the instrumentation was functioning properly. Table 1 shows a summary of the test conditions and measured data for various calibration runs.

3.2   Phase 2:   Corona Discharge Calibration

After completing the tunnel calibration phase, the TSI Corona Discharge Anemometer mounted on its stand was placed in the wind tunnel. As specified by ERC, the device was then calibrated by measuring its response to different known free stream conditions. The TSI's measurement of the components of velocity along V_x and across V_y the zero reference on the TSI were plotted with the chart recorder as a function of azimuth angle by using the motorized stand to rotate the device slowly 360° while monitoring its output. Azimuth angle, as well as the two velocity component signals filtered to remove electrical and turbulence-generated noise, were also plotted at the same time. This procedure was repeated for several combinations of velocity and turbulence intensity.

Next, the effect of pitch variation on the TSI anemometer readings was investigated by fixing the anemometer at a known pitch angle from the vertical

6

xz plane and again recording the x and y components of velocity on a chart recorder as the model rotated. The difference between these readings and the zero pitch angle measurements gave an indication of the effect of flow angularity on the accuracy of the TSI measurements. Table 2 presents a summary of the data taken during this phase of testing.

3.3   Phase 3:   Corona Discharge Anemometer Dynamic Velocity Measurements

To determine the ability of the TSI anemometer to determine accurately the characteristics of a turbulent velocity field, it was decided to compare its output with that of a hot wire placed outside of but in a position similar to the TSI's test section. All tests were performed at a fixed azimuth angle using the instrumentation previously described to monitor the outputs of the two devices. Simultaneous measurements of the turbulence intensity and frequency spectra made by the hot wire and TSI showed differences in some cases.

To find if these differences were caused by some fault in the electronics of the TSI or if they represented an accurate measurement of a velocity field modified by the TSI geometry, the procedure was repeated with the hot wire positioned inside the TSI's test channel. Turbulence intensity and frequency spectra were again measured for different hot wire positions.

The measurements made with the hot wire placed inside the TSI showed that the internal flow was in fact very different from that in the free stream and varied strongly with position inside the device. Thus, the readings from the TSI represented an average over the volume of the test section of a very complicated velocity field that in some cases varied greatly from the free stream. While only a few internal readings were made in this testing phase, two important aerodynamic problems were suggested by the hot wire velocity and frequency spectrum measurements: (1) leading edge separation was probably modifying the velocity field and introducing turbulent energy at a braod range of frequencies and (2) vortex shedding from the posts supporting the test section was introducing energy at a specific frequency determined by the Strouhal number of the cylindrical rods, causing a bump in the frequency spectra measurements. A summary of the data from this phase is presented in Table 3.

3.4   Phase 4:   Full-Scale Corona Discharge Model

A full-scale model of the corona discharge anemometer to be used by AFGL with a 1" gap and a slightly rounded leading edge was used to perform a more

detailed investigation of the internal velocity field of the device. All tests were performed with the model rigidly mounted near the rear of the tunnel test section. The turbulence generating grid was removed and the low speed, low turbulence fan used for all runs. Thus, any nonuniform flow in the device and any change from the free stream frequency spectrum and/or turbulence intensity would be mainly due to aerodynamic effects of the device.

A movie made of the initial smoke studies was used to determine visually possible trouble areas in the device. Next, the internal velocity field was surveyed by first positioning the hot wire at a desired height from one of the flat surfaces of the cylinders forming the test section of the anemometer and even with the trailing edge, then moving it forward in eight evenly spaced increments toward the leading edge.

This procedure was repeated for each new height to deduce the flow pattern in the plane parallel to the free stream and bisecting the model longitudinally. For most hot wire surveys, the model was oriented so that the supporting posts straddled the center line and, therefore, the hot wire was not normally placed immediately in their wake. A few points were taken, however, with the hot wire positioned directly in the wake of a post.

Most tests were conducted with the hot wire axis mounted vertically, but the few runs that were repeated with a horizontally-mounted hot wire showed no significant changes in the readings.

3.5   Phase 5: Modified Corona Discharge Model

As a result of the information found in Phase 4, a second model with greatly increased leading edge radius was constructed. It was hoped that this change would decrease leading edge separation, and thus would improve the accuracy of the instruments frequency spectrum measurements. Testing procedures were identical to those of Phase 4. Movies were first made in a smoke-visualization study of the model at different angles of attack to attempt to determine empirically if the model had in fact reduced separation. Internal velocity surveys and frequency spectrum measurements were then made to find if the ability of an actual device to measure the free stream flow should be expected to be improved by the modifications used in this model.

8

SECTION 4

RESULTS

4.1   Phase 1:   Wind-Tunnel Calibration

A total of the thirteen calibration runs was made to define the tunnel conditions with no model present.   These tests are summarized in Table 1, which lists the experimental set-up and reduced data from each run.   Figures 6 through 17 are the corresponding composite plots of frequency spectra squared taken during these runs.

The composite plots were formed by combining several of the plots for various frequency ranges made by the ubiquitous spectrum analyzer.   An average of three to five plots were generally used to construct each composite curve.   At the low frequency range only 32-64 spectrum averages could be taken, resulting in considerable scatter in the data.   Most of this scatter in the signal was smoothed while constructing the composite plots; however, significant peaks were always retained.   The -5/3 slope line indicated on each curve represents the slope with which the theoretical von Karman spectrum would decay at high frequencies.   The relative magnitude of the individual frequency spectra plots at a frequency of 1 Hz can be found by comparing the size of the quantity (velocity x turbulence intensity)^2 for each run.   This quantity is inversely proportional to the amplification used to produce the plot and, therefore, also serves as an indication of the relative signal-to-noise ratios for various runs.

Besides serving as reference data for later frequency analysis, the composite plots, Figs. 6 through 17 made from the tunnel calibration data illustrate several trends predicted by theories of turbulent flow.   Figures 6 through 9, for example, show the results of four runs made at different velocities but at the same downstream location.   As expected, the tangent point between the frequency spectra curves and a $-45°$ line (which can be considered to indicate approximately the frequency that contains the largest amount of energy in the flow) moves toward lower frequencies as the velocity decreases.   It is also important to note the increasing size of the spikes caused by electrical and mechanical noise that appear on the plots as velocity decreases.   These can be explained easily by noting that much higher amplification is needed to obtain a usable signal from the low energy (low speed) flows; thus, the

9

signal-to-noise ratio decreases with velocity and the magnitude of the
electrical and tunnel generated aerodynamic noise in the system begins to
dominate the plots, especially at the high frequencies which, in general,
contain only a small fraction of the energy in a flow. This effect should
be kept in mind when interpreting all the frequency spectra data presented
in this report.

Figures 7, 11 and 12 illustrate the fact that the high frequency gusts
will decay at a faster rate than those of lower frequencies. These three runs
were conducted at approximately the same velocity but at different distances
and, therefore, different lengths of time downstream from the grid. The
peak-energy-containing frequency is again illustrated by the intersection
of a $-45°$ slope line and the composite frequency curve. Because of the
rapid dissipation of high frequency gusts, this intersection tends to move
to lower frequencies as the distance downstream increases, showing that a
larger percentage of the energy present is contained in the low frequencies
farther from the grid.

The noise level in the WBWT is very high when the main motor is used
for driving the flow. The effect of this noise on the frequency spectra is
illustrated by Figs. 14 and 15. These figures show that the noise from the
propeller appears to fall mostly in the 8-100 Hz range. For flow at low
speed (Fig. 15) the usual spectra, with the expected -5/3 drop off with
frequency, can be seen below 8 Hz, with the noise dominating the spectrum at
higher frequencies. At higher speed (Fig. 14) the spectrum is almost completely
obscured by the tunnel noise. Using the low speed fan, which produces very
little noise, the frequency spectra are now much more like the expected -5/3
curves since the signal-to-noise ratio has been substantially increased
(Figs. 16 and 17).

4.2   Phase 2: Corona Discharge Calibration

This phase of testing was intended to determine the ability of the
Corona Discharge Anemometer to measure the average velocity components of the
free stream flow. The nine test runs listed in Table 2 were made specifically
for this purpose. As initially planned, the static calibrations were to be
done by reading the TSI's velocity components at fixed increments of rotation;
however, this procedure was abandoned after the first run in favor of continuous
measurement by producing velocity versus angle plots with the chart recorder.
Figures 18 through 20 are representative of these plots.

10

Figure 18 shows a typical plot for a low velocity run. The first two curves (1 and 2) of this figure are plots of the unfiltered V_x and V_y components of the TSI's output, while curve 3 shows the corresponding angle of inflow. Curves 4 and 5 show the same V_x and V_y components after being filtered (RC $\simeq$ .01 sec) to remove some of the electrical noise. Note that after passing through the two-to-one voltage divider in the filter circuit, the scale for the filtered signal is half that of the unfiltered one.

The variation in the size of the positive and negative peaks of the V_y component of velocity is most likely due to aerodynamic problems induced by the mounting stand supplied by ERC. The flat plate used to obtain an angle of attack on this stand is positioned perpendicular to the y axis just in front of and below the lower 3" cylinder. This plate might be expected to cause little or no disturbance to the flow in the x direction, but produce a non-symmetric influence on the y component of flow as the anemometer is rotated.

Figure 19 shows a similar result, this time at a higher speed. Note that the noise in the unfiltered signal is substantially less than in Fig. 18. With the better signal-to-noise ratio at this higher speed, variations in the velocity component versus angle plots become noticeable. These variations are thought to be caused by the wake of the supporting posts around the perimeter of the device, with the oscillations corresponding to the passage of the posts in front of the measuring section of the anemometer.

Figures 19 and 20 illustrate typical runs conducted to determine the effect of flow angularity out of the horizontal plane on the ability of the device to measure velocity. These plots, along with Figs. 20 and 21 show that variations in angle of attack up to 30° do not significantly change the ability of the TSI to measure the average free stream velocity.

Figures 21 and 22 are plots of free stream velocity components in the x and y directions versus the corresponding TSI outputs. These calibration curves were produced by measuring one half of the peak-to-peak voltage at each velocity from the chart recorder data. Both curves are reasonably linear; however, the V_y component should be regarded with some suspicion due to the previously described problems with the pitch angle plate on the mounting stand. The velocity acceleration evident inside the TSI instrument (see Figure 38) is not shown in Figures 21 and 22 since the TSI output was initially set to match wind tunnel velocity.

11

4.3   Phase 3:   Corona Discharge Anemometer Dynamic Velocity Measurements

A total of 17 runs was made to determine the dynamic response of the Corona Discharge Anemometer.   The conditions for these runs and the data taken are listed in Table 3.   Figures 23 through 37 are the corresponding composite plots of frequency spectra squared for these runs.   These frequency spectra curves should not be considered as a quantitative measure of the TSI's performance; they should be used only as a qualitative guide for interpreting the data obtained in any testing done by AFGL using the anemometer. By comparing the TSI output curves with those made for similar conditions during the calibration phase, some feeling for the response of the device in different situations can be attained.   Since the value of these calibration curves depends on the intuition of the investigator, no attempt will be made to explain each one in detail; however, important trends will be pointed out.

Figure 23 is an example of a plot illustrating one of the major problems with the anemometer as supplied by AFGL for testing: an obvious bump centered at about 40 Hz has appeared in the frequency spectrum.   This bump indicates that energy at a fairly broad band of frequencies has been introduced on top of the free stream spectra.   Later investigation showed that this phenomenon was due to leading edge separation at the entrance to the test section.   This effect can be seen to some degree in a large number of the composite plots, with the position of the bump changing with velocity.

A second, less consistent, phenomenon may explain some of the spikes appearing on the curves.   It is well known that at certain Reynolds numbers, the wake of cylindrical objects placed in a flow will exhibit oscillations at a specific frequency predicted by the Strouhal number.   The frequencies predicted by this method for the wake shed by the supporting posts of the anemometer are in close agreement in some cases with spikes in the frequency spectrum.   Run 23 was conducted with one of the supporting posts was directly in front of the corona. Run 22 was conducted with the corona aligned between two supporting posts.

By selecting the appropriate curves, the measured response of the TSI as a function of many different parameters can be deduced from the information in these curves.   Data are available to make direct comparisons of the effect of velocity, downstream distance, turbulence intensity, and angle of attack, among other possibilities.   Figure 25 shows a plot produced with the entrance to the TSI covered to find the zero velocity frequency spectra of the device, a measure of the noise in the system.   Figures 34 through 37 which show several composite frequency spectrum plots from both the hot wire and TSI on the same graph, are especially useful in comparing spectra from the device with that in the free stream.   For example, comparison of curves a and b in Fig. 37 clearly shows the bump in the spectra due to leading edge separation.

12

4.4   Phase 4:   Full-Scale Corona Discharge Model

This phase of testing was conducted using a full scale model of the Corona Discharge Anemometer. A hot wire was used to survey the velocity field inside the model at various distances above and below the centerline. The results of these surveys are shown in Figs. 38a and 39a. Figure 38a, a plot of the velocity ratio at various heights in the model, suggests that the front third of the test channel is a region of separated flow. The plot of the turbulent intensity as a function of position in the model, Fig. 39a, shows that a large amount of turbulence has been introduced near the lower surface, indicating that it is the lower edge that has separated. These figures tend to be confirmed by the movies of smoke studies.

Figure 40 is a plot of the free stream spectrum at the test conditions, while Figs. 41 through 44 are the spectra at points at, above, and below the center of the model's test channel for the same conditions. Comparison of the interior plots with the free stream curve shows the obvious bump in the spectrum due to the leading edge separation. This added energy has in fact prevented the interior curves from falling off at the theoretically predicted -5/3 slope and almost completely masked the free stream spectrum. These curves indicate that it is important to consider the relative signal-to-noise ratio and the frequency range in question when interpreting the frequency spectra curves, especially when comparisons are being made between two or more plots made at different velocities or turbulence intensities.

These curves also show that the flow field inside the device is a strong function of position. Comparison of Figs. 41 and 42 illustrate this clearly. The Corona Discharge Anemometer will tend to measure the average across the test section of a flow which has been shown to differ significantly from the free stream. This point to point difference in flow characteristics inside the device could in some cases lead to completely wrong measurements by the TSI.

It should be noted that the two spikes which appear above 100 Hz in Figs. 42 and 43 may be examples of vortex shedding from the posts as mentioned in the previous section.

4.5   Phase 5:   Modified Corona Discharge Model

A second model was built to attempt to eliminate the leading edge separation problem. This model was tested in the same manner as the model

13

in Phase 4. Figures 38b and 39b show the velocity ratio and turbulence
intensity curves resulting from the internal hot wire measurements. Com-
parison of these plots with Figs. 38a and 38b indicate that, while the
interior flow has been accelerated due to the convergent nozzle shape of
the inlet, the turbulence intensity is reduced and the separation is less
severe.

Comparison of Figs. 45 and 47 taken at the positions indicated on the
plots shows that the reduction in leading edge separation has not eliminated
the bump in the frequency spectrum; however, the turbulence intensity is much
less (see Fig. 39). The two curves do, however, agree more closely with the
free stream spectrum, Fig. 40, than those produced with the original model.
It seems likely that the bump is caused by a small separation that has
reattached. Figures 46 and 47 show the spectra produced at identical condi-
tions by the hot wire in two different orientations: in 46 the hot wire was
mounted vertically, while in Fig. 47 it was mounted horizontally. The
similarity of the two curves indicates that the orientation of the hot wire
was probably not of major importance in the measurements taken during the
program.

REFERENCES

1. Baines, W. D. and E. G. Peterson, "An Investigation of Flow through
   Screens", Transactions of the ASME, July 1951, pp. 467-480.

TABLE 1

WIND TUNNEL CALIBRATION DATA

RUN	FIGURE	MOTOR	GRID	VELOCITY (m/sec)	TU(%)	X(m)
1	6	MAIN	IN	13.23	5.5	4.57
2	7			6.86	7.3	4.57
3	8			3.41	5.0	4.57
4	9			1.55	3.1	4.57
5	10			1.98	8.8	1.98
6	11			6.77	16.7	1.98
7	12			6.79	25.9	0.82
8	13		IN	1.95	19.2	0.82
9	14		OUT	5.58	2.4	4.57
10	15			0.73	1.29	4.57
11	--	MAIN		2.25	3.2	4.57
12	16	FAN		3.44	0.60	4.57
13	17	FAN		0.73	0.56	4.57

TABLE 2

CORONA DISCHARGE AVERAGE VELOCITY CALIBRATION

RUN	FIGURE	VELOCITY (m/sec)	TU(%)	X(m)	TSI V_x (VOLTS)	TSI V_y (VOLTS)	CONDITIONS
15	--	3.35	--	4.57	--	--	TSI Velocity Cal. at Fixed θ Positions
16	--	3.41	0.60	4.57	0.360	0.370	Velocity Cals. Using
17	--	2.07	0.45	4.57	0.220	0.215	Chart Recorder and
18	--	1.07	0.28	4.57	0.113	0.115	Continuous θ Rotation
19	--	0	0	4.57	0	0	Measurement of 0 Velocity
20	18	0.58	0.43	4.57	0.068	0.065	Same as Run 16
21	--	0.73	0.32	4.57	0.085	0.088	
25	--	3.17	0.55	4.57	--	--	
28a	--	3.20	0.86	4.57	0.330	0.330	Effects of Tilt 0°
28b	19	3.20	0.81	4.57	0.315	0.330	$+30^{\circ}$ (Up)
28c	--	3.20	0.88	4.57	0.315	0.330	-30° (Down)
28d	--	3.20	0.83	4.57	0.325	0.330	-20° (Down)
28e	20	3.20	0.83	4.57	0.330	0.330	-10° (Down)

ALL RUN WITH NO GRID AND LOW TURBULENCE FAN

TABLE 3

CORONA DISCHARGE FREQUENCY SPECTRUM DATA

RUN	FIGURE	VELOCITY (m/sec)	TU(%)	X(m)	TSI V_x (VOLTS)	TSI V_y (VOLTS)	CONDITIONS
22	23	3.14	0.51	4.57	0.330	0.330	Spectrum at Peak of Oscillation of Chart Recorder
23	24	3.14	0.60	4.57	--	--	Same in Valley
24	25	0	--	4.57	--	--	TSI Inlet Covered
26	--	3.17	0.55	4.57	--	--	Repeat of 22
27	26	2.68	0.56	4.57	0.330	0.330	Repeat of 22 at Lower Velocity
29	27	3.20	0.86	4.57	--	--	Spectra at -30° Tilt
30	28	10.91	--	4.57	1.090	1.125	Frequency Spectra
31	29	2.80	5.4	4.57	0.295	0.290	Frequency Spectra
32	--	9.91	6.4	4.57	1.00	--	V_x RMS = .050 Volts
33	30	9.51	7.1	4.57	--	--	Hot Wire Inside TSI (Spectra)
34	31	9.39	6.7	4.57	--	--	Hot Wire In Free Stream (Spectra)
35	32	3.72	5.1	4.57	--	--	Hot Wire in Free Stream
36	33	3.72	8.3	4.57	--	--	Hot Wire in TSI
37a	34	1.55	1.93	1.98	0.185	.180	Hot Wire in Free Stream
37b	34	1.62	1.93	1.98	--	--	TSI Spectrum
37c	34	1.65	1.71	1.98	--	--	Hot Wire in TSI
38a	35	10.61	11.1	1.98	1.10	1.125	Hot Wire in TSI
38b	35	10.36	15.5	1.98	--	--	Hot Wire in Free Stream
38c	35	10.55	14.9	1.98	--	--	TSI Spectrum
39a	36	8.96	10.5	1.98	1.00	1.075	30° Tilt-Hot Wire in TSI
39b	36	--	12.1	1.98	--	--	Hot Wire in Free Stream
39c	36	9.91	11.9	1.98	--	--	30° Tilt-TSI Spectrum
40a	37	3.14	0.59	1.83	--	--	TSI Spectrum
40b	37	3.14	0.63	1.83	--	--	Hot Wire in Free Stream
40c	37	3.14	2.30	1.83	--	--	Hot Wire in TSI
40d	37	3.14	1.08	1.83	--	--	Hot Wire Forward of Center in TSI

NOTE: V_x and V_y VOLTAGES TAKEN FROM CHART RECORDER AVERAGES

25'-1".

73'

15'

10'

7'-6"

Instrument Panel

17
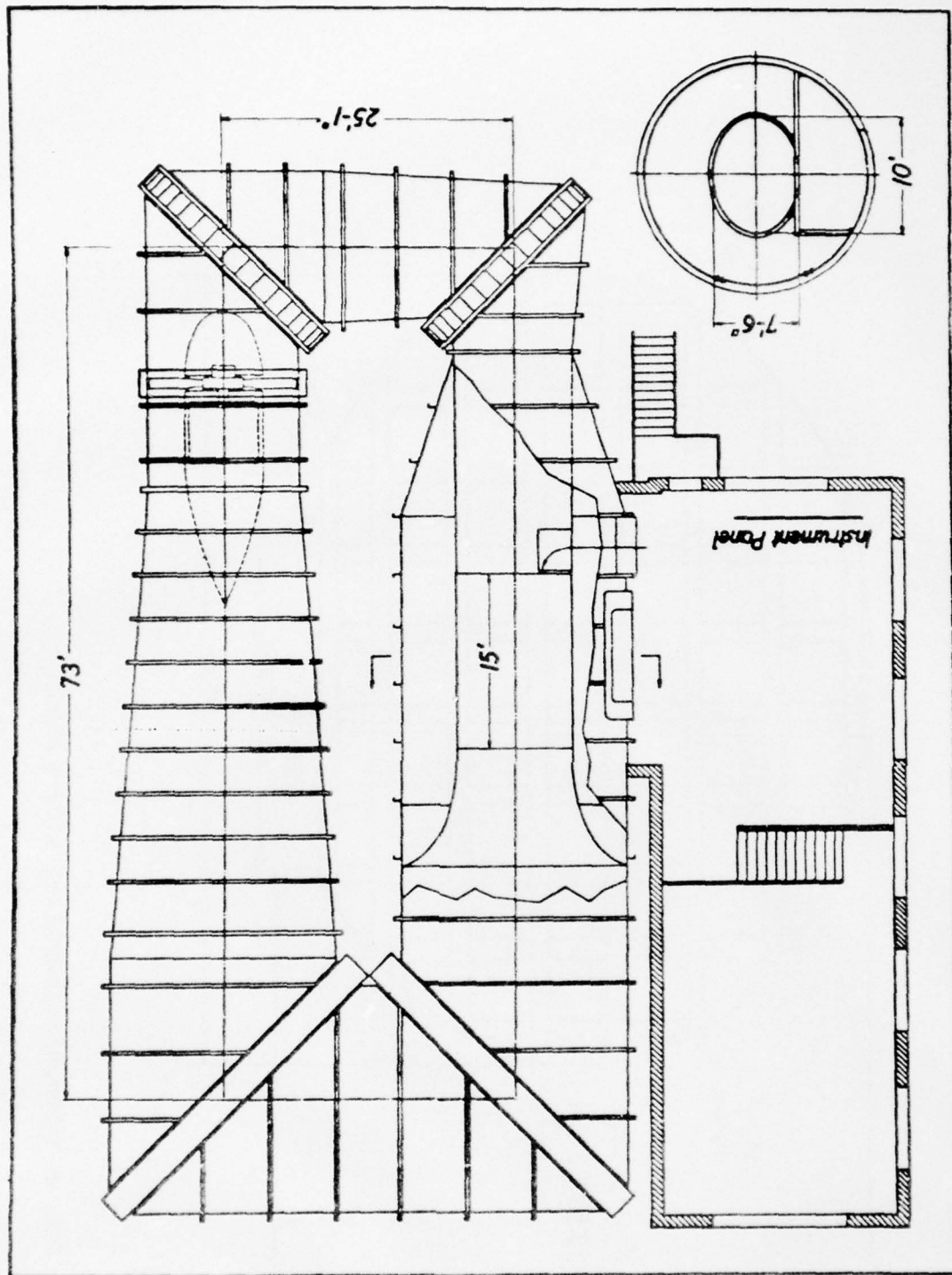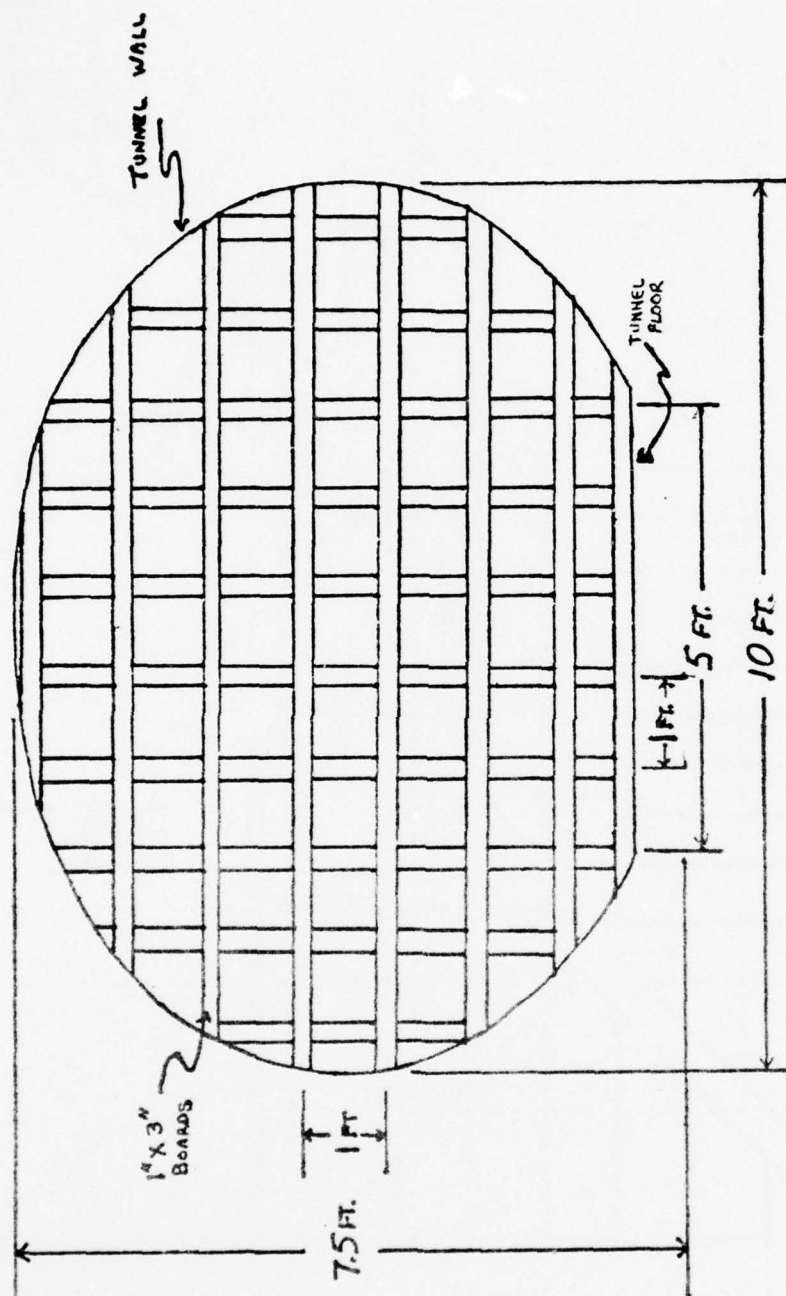
FIG. 2 TURBULENCE GENERATING GRID IN TUNNEL

18

(1/32 INCH EDGE RADIUS)

X-AXIS

Y-AXIS

22.5°

1/16 DIA

2.75"

3.0"

2.25"

.5

1/32" RADIUS
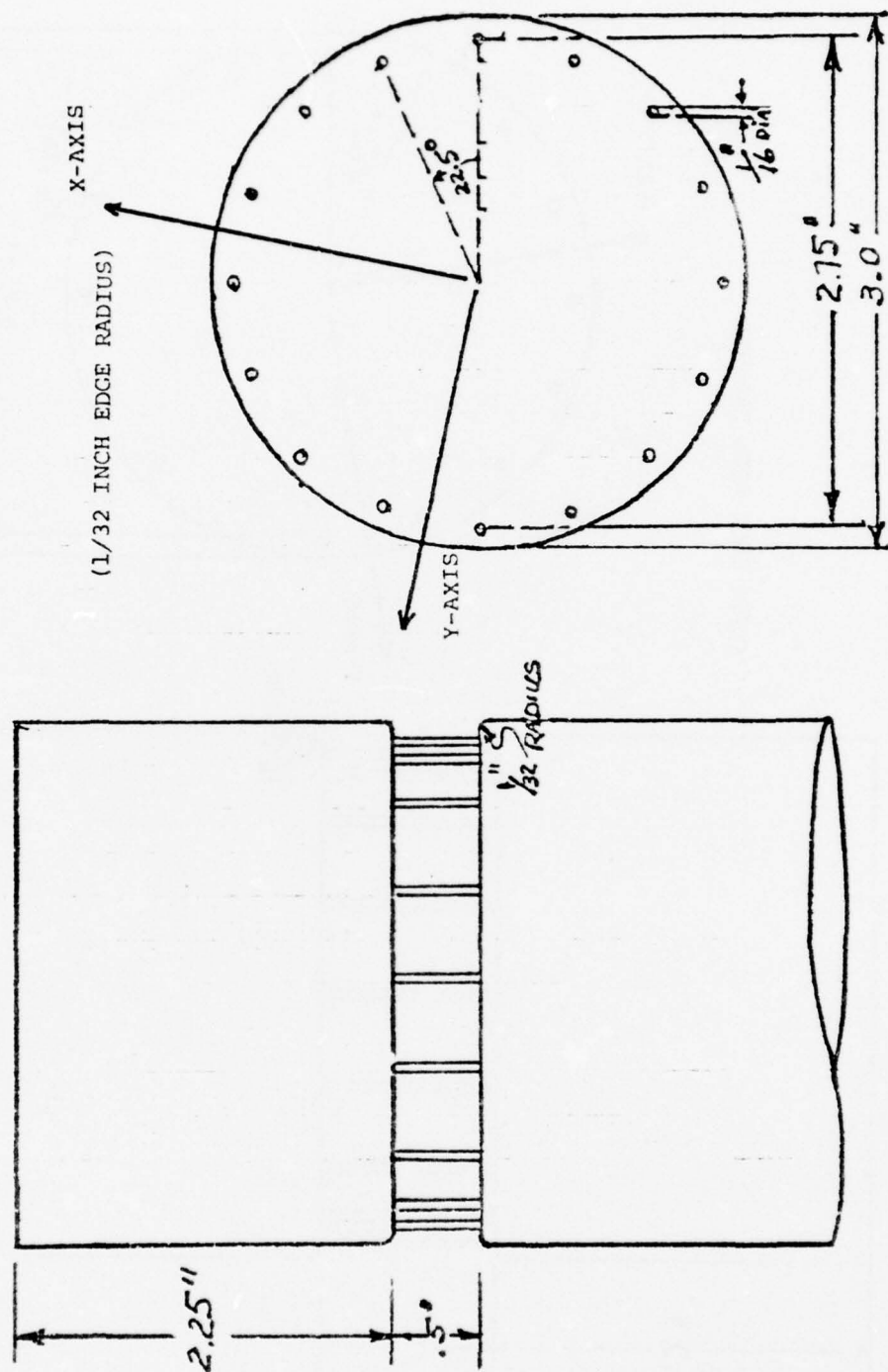
FIG. 3 CORONA DISCHARGE ANEMOMETER

19

(1/16 INCH EDGE RADIUS)

X-AXIS

22.5°

Y-AXIS

1/16" DIA.

2.75"
3.0"

1/16" RADIUS

2.25"

1"
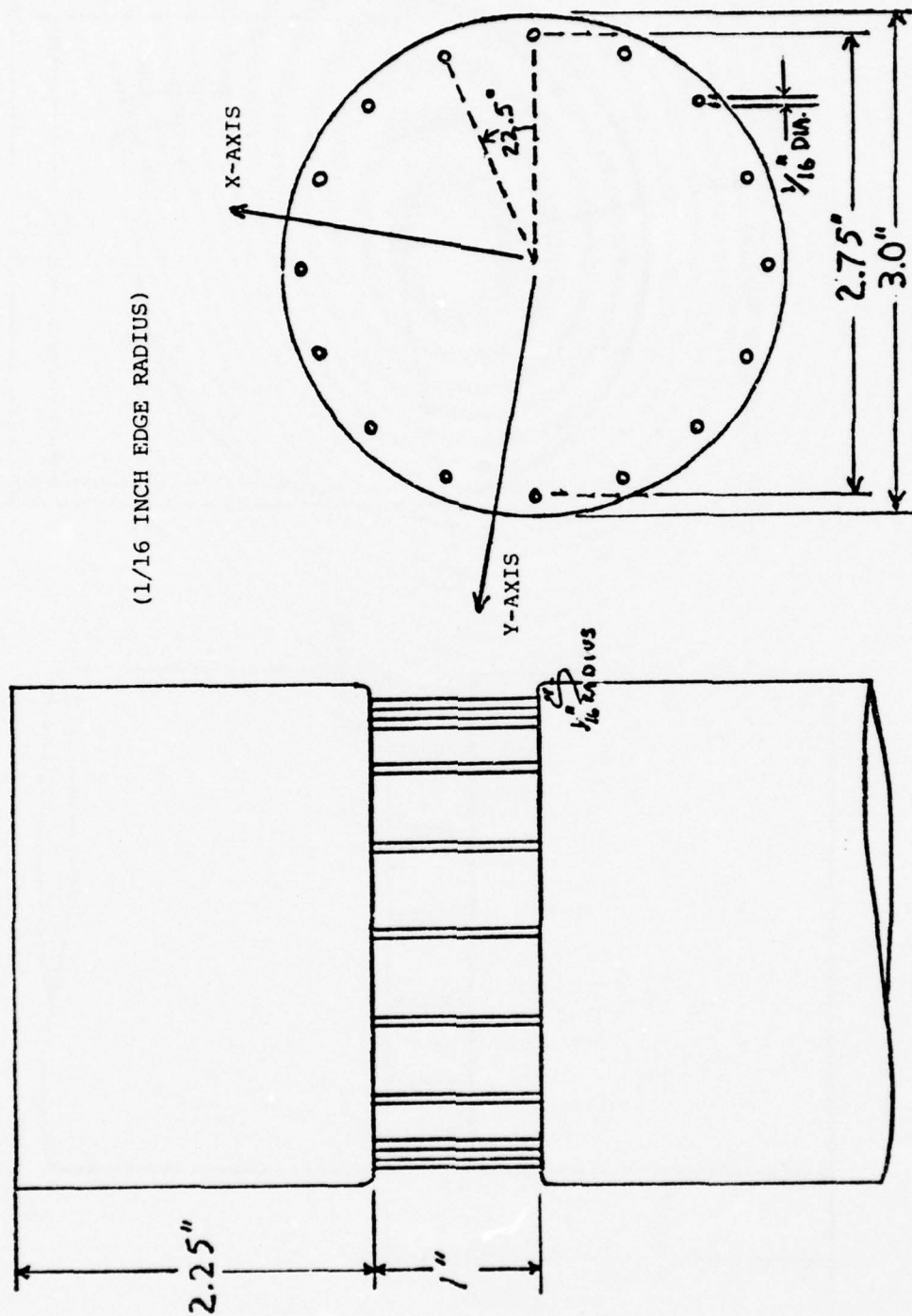
FIG. 4 FIRST FULL-SCALE MODEL OF THE CORONA DISCHARGE ANEMOMETER

20

(1/2 INCH EDGE RADIUS)

X-AXIS

2.75

Y-AXIS

3.0"

2.75"

$\frac{1}{16}$OIA

1/2" RAD.

2.75"

1.0"

FIG. 5 SECOND FULL-SCALE MODEL OF THE CORONA DISCHARGE ANEMOMETER

21

MAIN MOTOR
4.57 METERS FROM GRID
V = 13.2 m/sec   Tu = 7.3%

5/3

-1

FREQUENCY (Hz)

S(m) (V²/m)
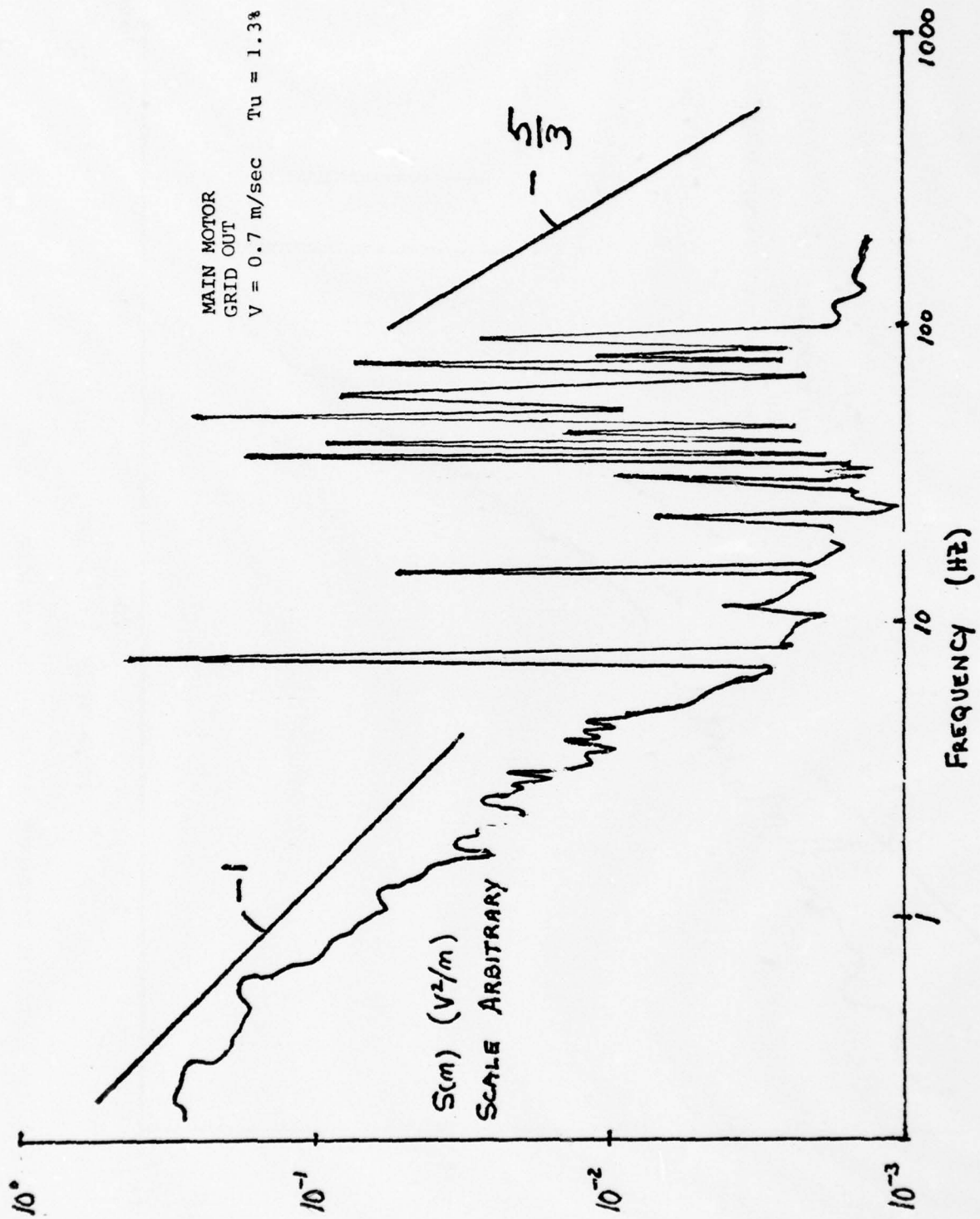SCALE ARBITRARY

10^0

10^{-1}

10^{-2}

10^{-3}

1

10

100

1000
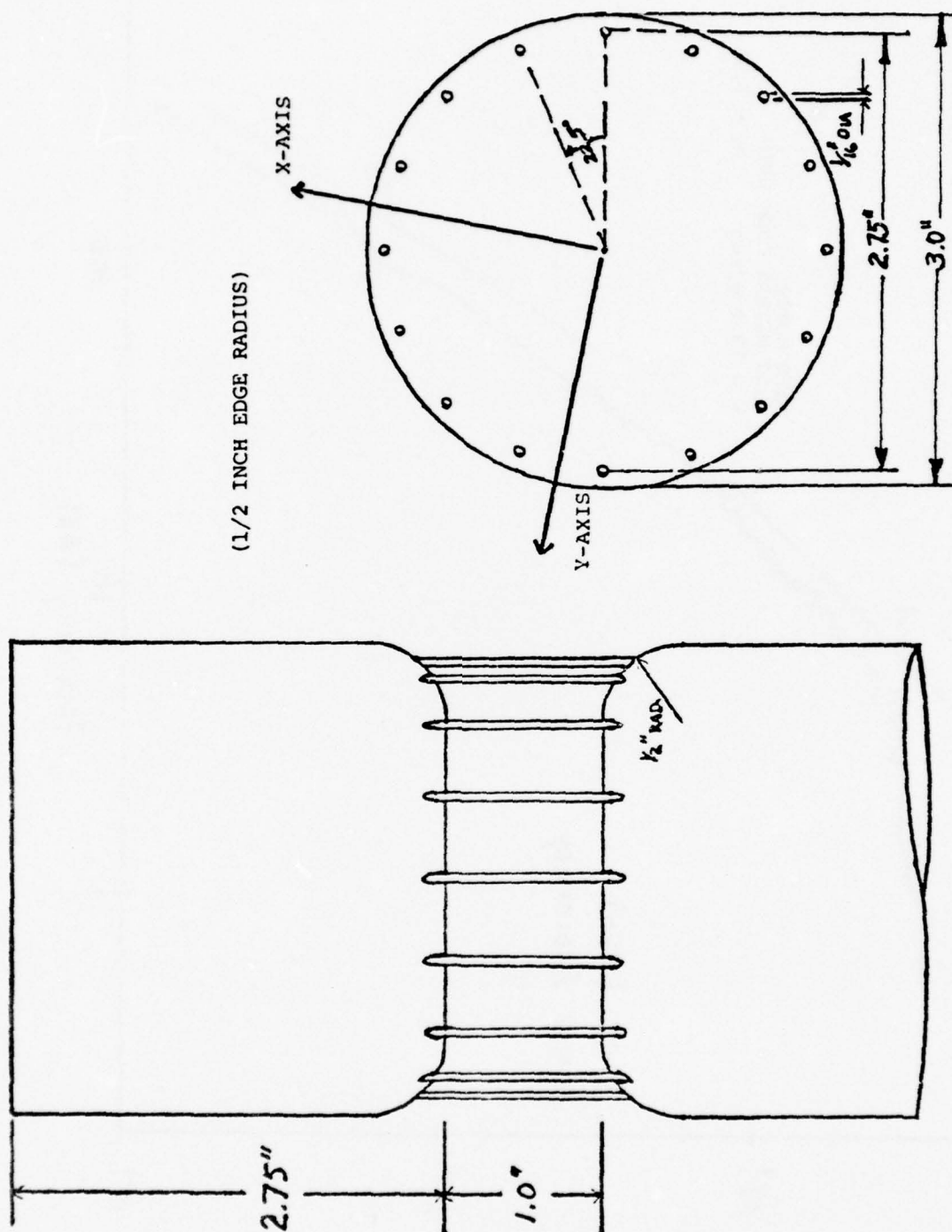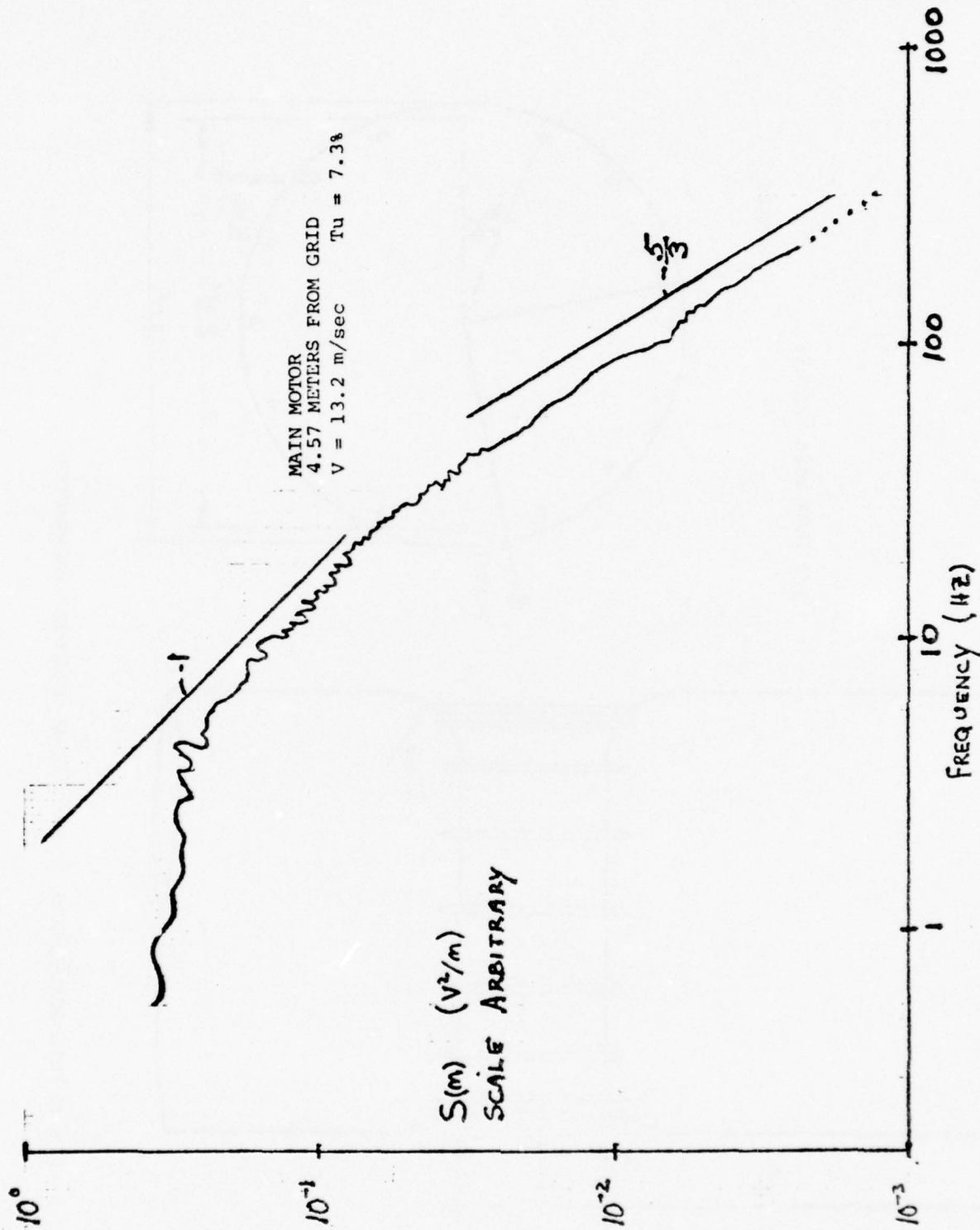
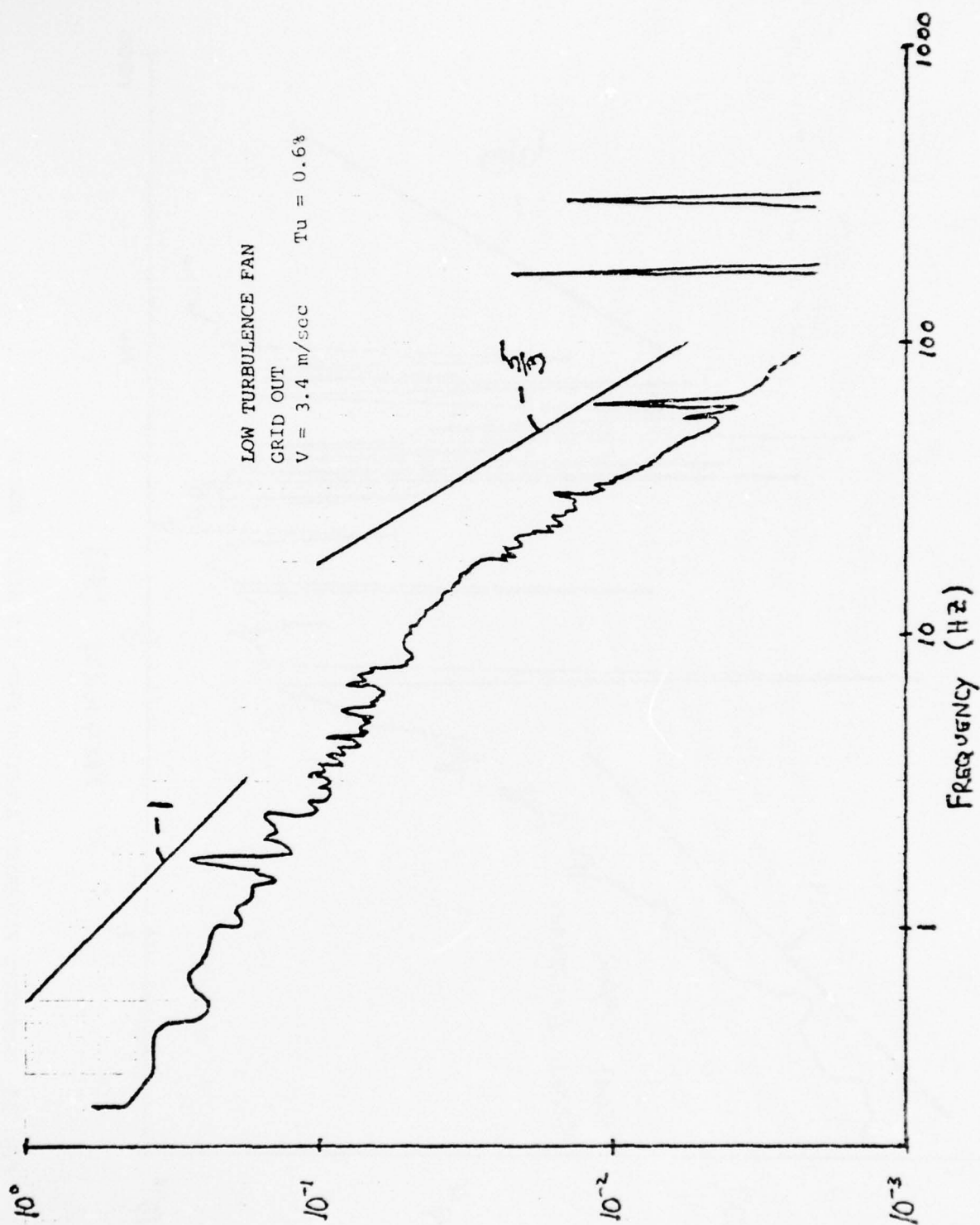FIG. 6 COMPOSITE FREQUENCY SPECTRUM FROM HOT WIRE - RUN 1

22

FIG. 7 COMPOSITE FREQUENCY SPECTRUM FROM HOT WIRE - RUN 2

MAIN MOTOR
4.57 METERS FROM GRID   Tu = 7.3%
V = 6.9 m/sec

$S(n) (V^2/m)$
SCALE ARBITRARY

FREQUENCY (Hz)

MAIN MOTOR
4.57 METERS FROM GRID   Tu = 5.0%
V = 3.4 m/sec

~60 Hz

$-\frac{5}{3}$

FREQUENCY (Hz)

S(m) (V²/m)
SCALE ARBITRARY
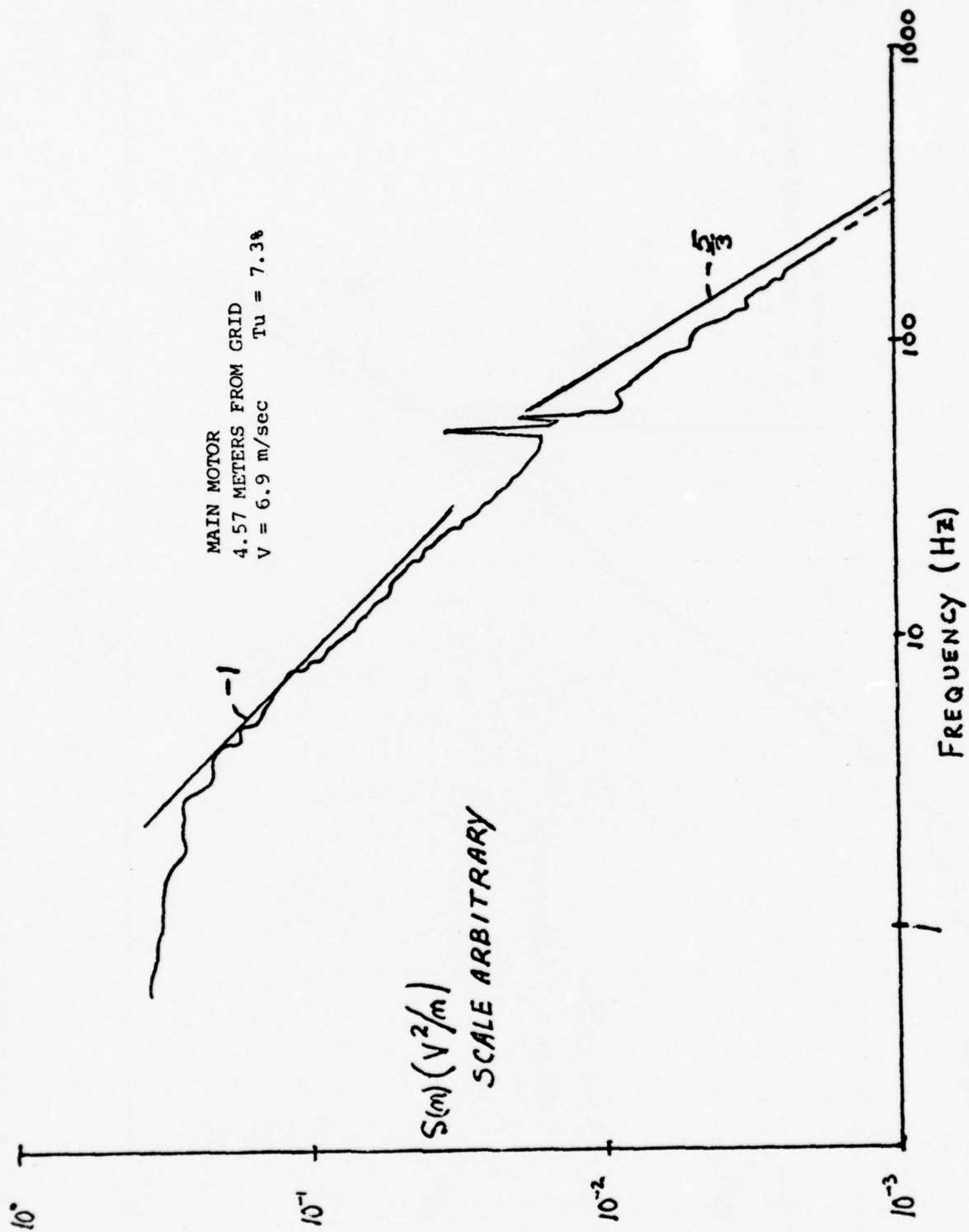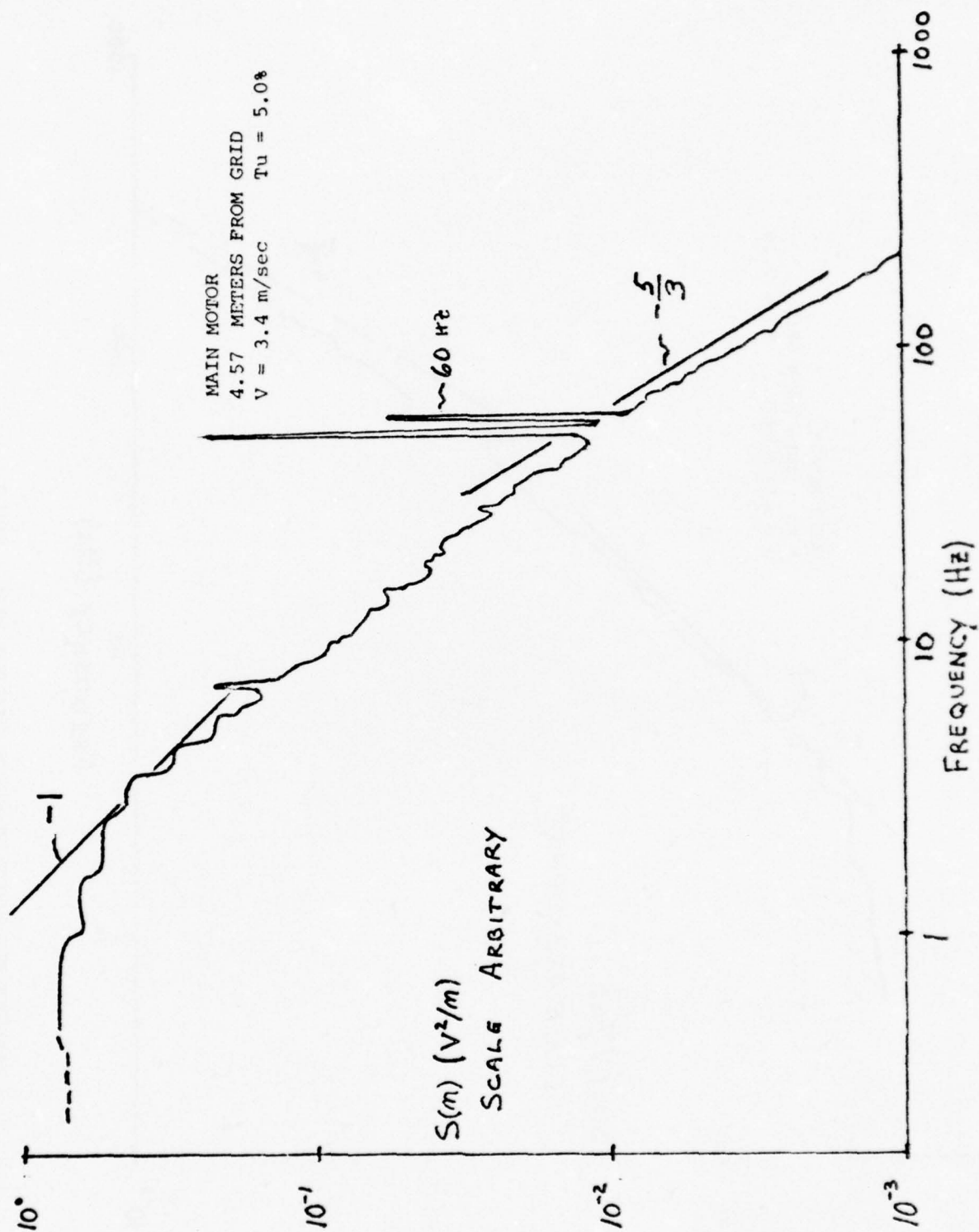
FIG. 8 COMPOSITE FREQUENCY SPECTRUM FROM HOT WIRE ~ RUN 3

24
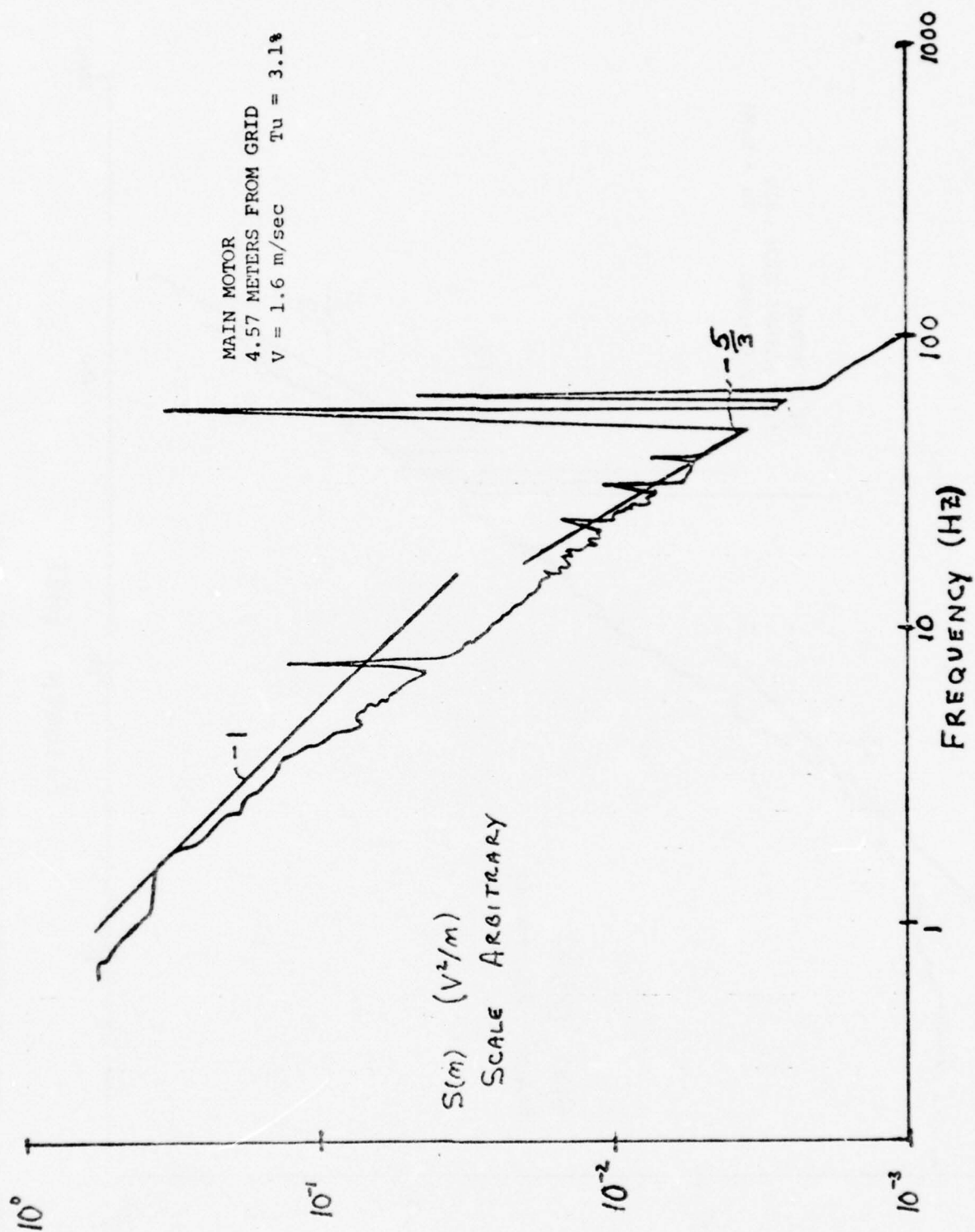
FIG. 9 COMPOSITE FREQUENCY SPECTRUM FROM HOT WIRE - RUN 4

25

FIG. 10 COMPOSITE FREQUENCY SPECTRUM FROM HOT WIRE - RUN 5

26

MAIN MOTOR
1.98 METERS FROM GRID
V = 6.8 m/sec   Tu = 17%

S(n), (V²/m)
SCALE ARBITRARY
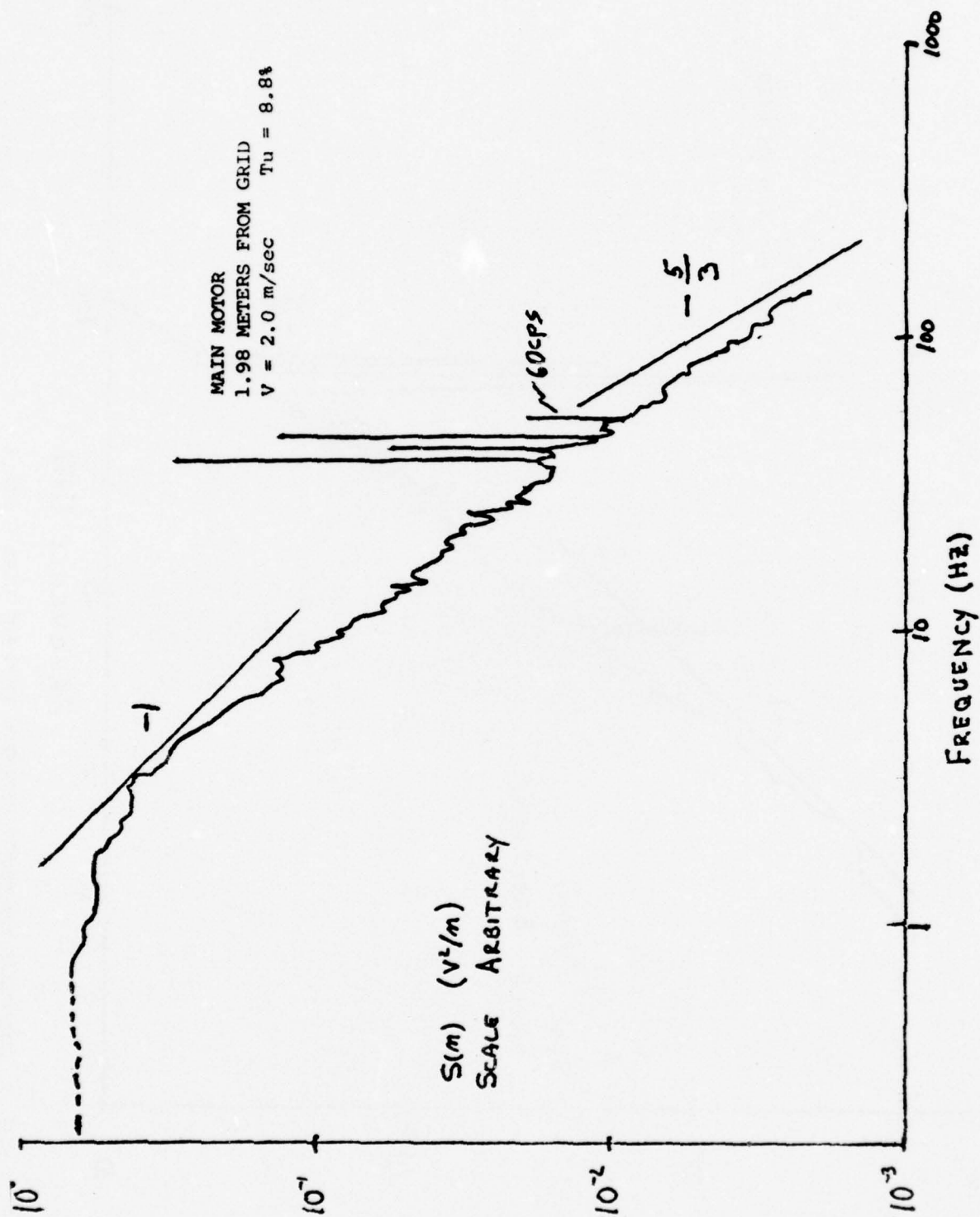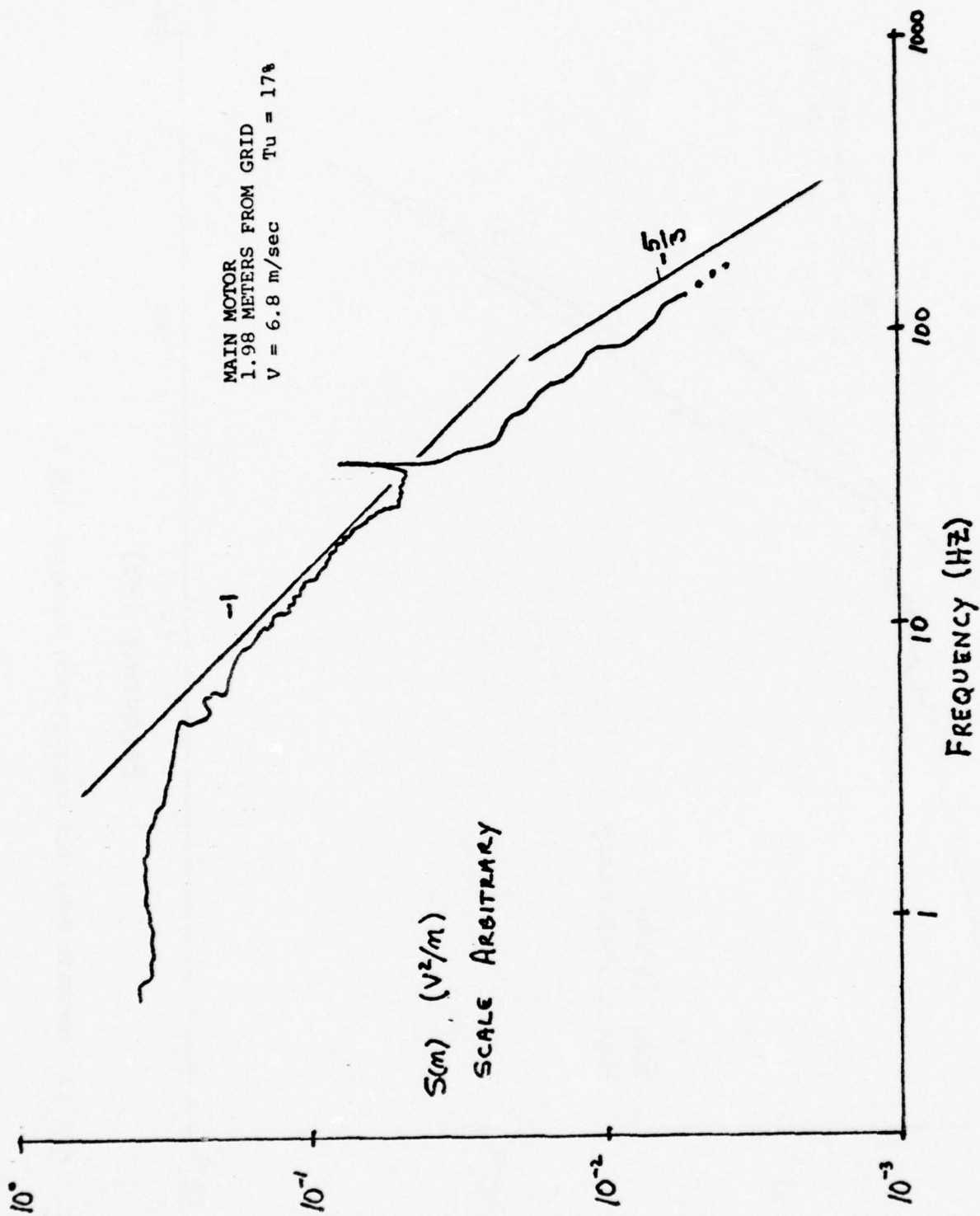
FIG. 11 COMPOSITE FREQUENCY SPECTRUM FROM HOT WIRE - RUN 6

27

FIG. 12 COMPOSITE FREQUENCY SPECTRUM FROM HOT WIRE - RUN 7
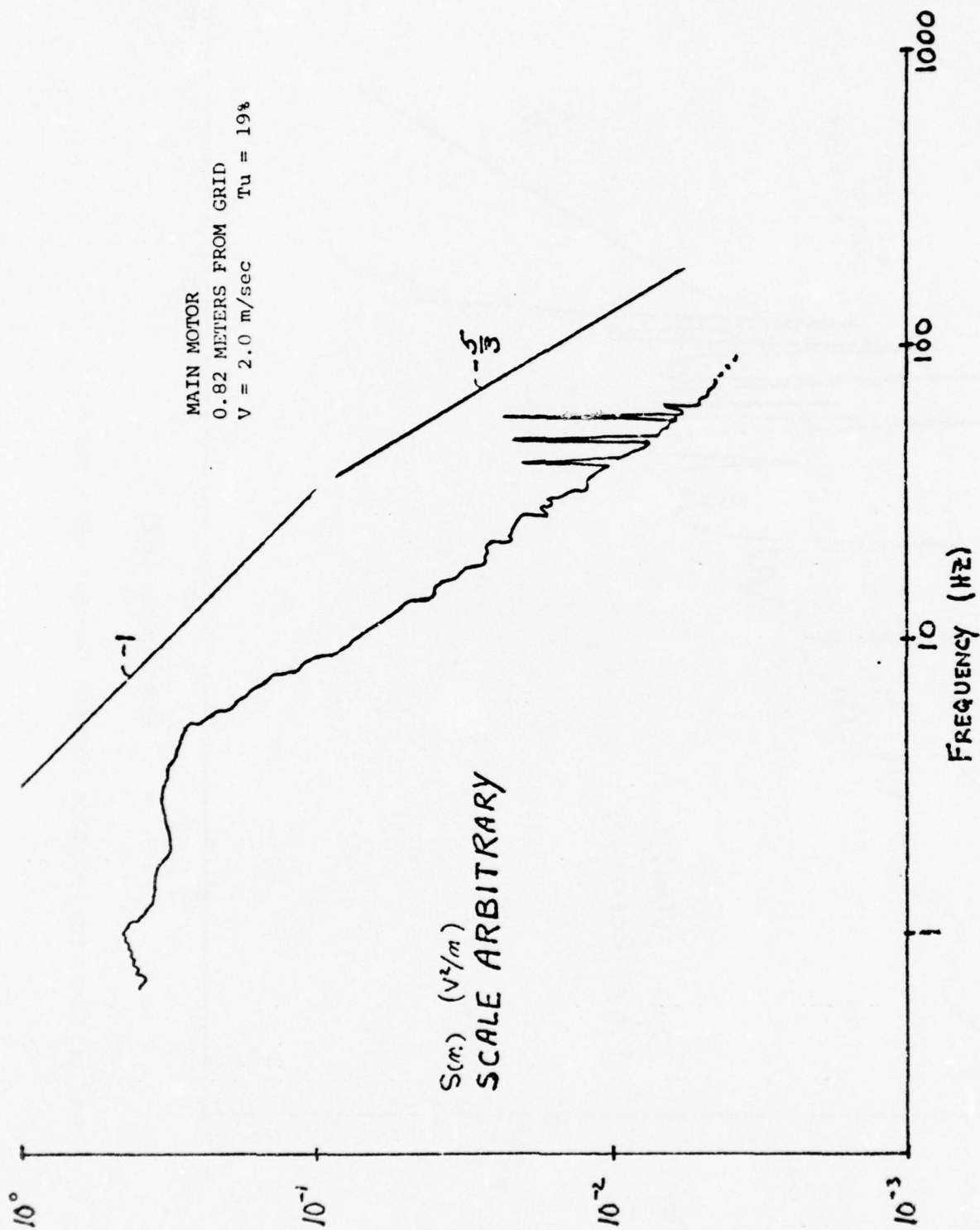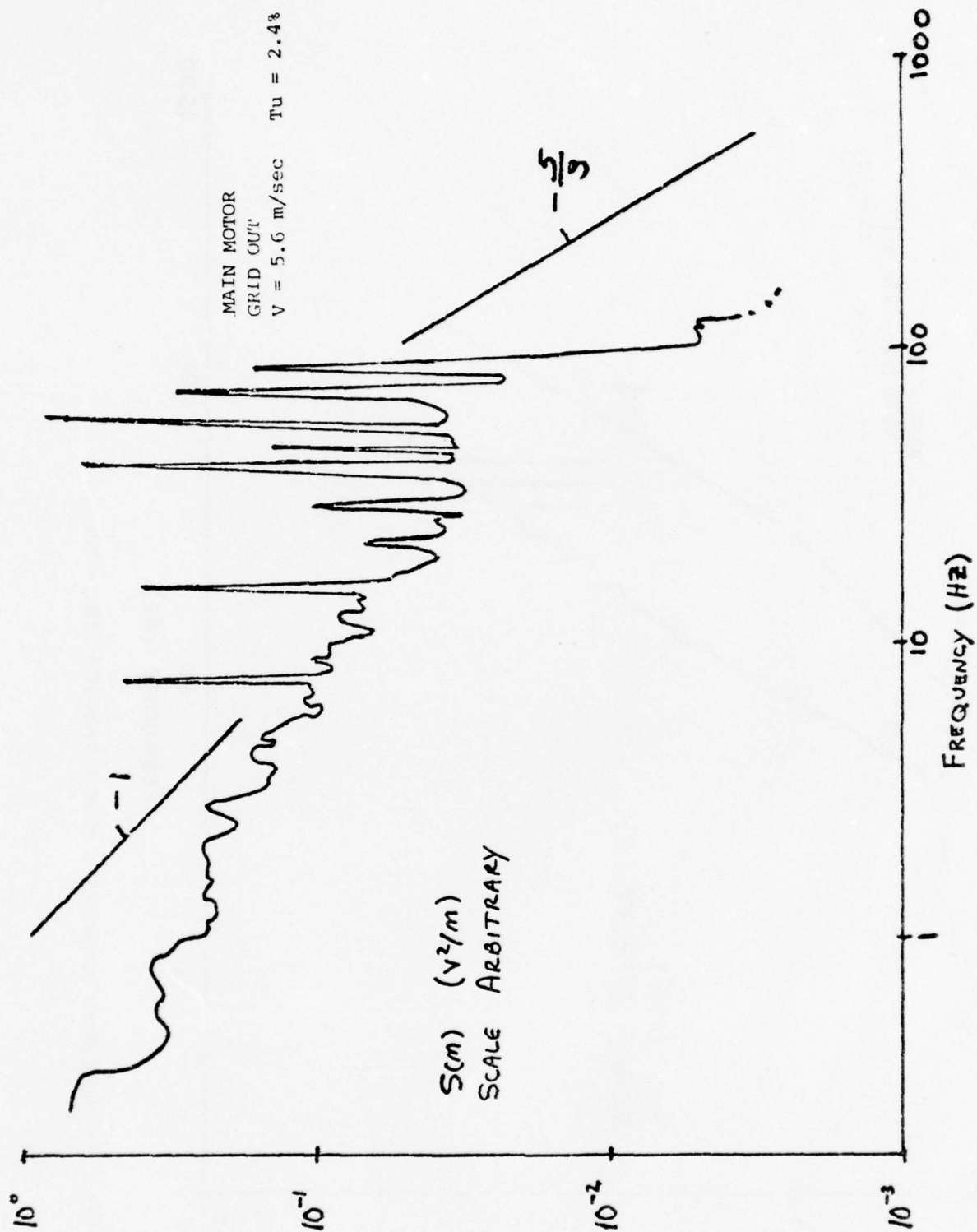
MAIN MOTOR
0.82 METERS FROM GRID
V = 2.0 m/sec   Tu = 19%

FIG. 13 COMPOSITE FREQUENCY SPECTRUM FROM HOT WIRE - RUN 8

29

MAIN MOTOR
GRID OUT
V = 5.6 m/sec   Tu = 2.4%

$-\frac{5}{3}$

-1

S(m) (v^2/m)
Scale Arbitrary

FREQUENCY (HZ)

10^0

10^{-1}

10^{-2}

10^{-3}

1

10

100

1000

FIG. 14 COMPOSITE FREQUENCY SPECTRUM FROM HOT WIRE – RUN 9

MAIN MOTOR
GRID OUT
V = 0.7 m/sec   Tu = 1.3%

5/3

-1

S(ω) (V²/m)
SCALE ARBITRARY

FREQUENCY (Hz)

FIG. 15 COMPOSITE FREQUENCY SPECTRUM FROM HOT WIRE - RUN 10

LOW TURBULENCE FAN
GRID OUT
V = 3.4 m/sec   Tu = 0.6%

FIG. 16 COMPOSITE FREQUENCY SPECTRUM FROM HOT WIRE - RUN 12

32
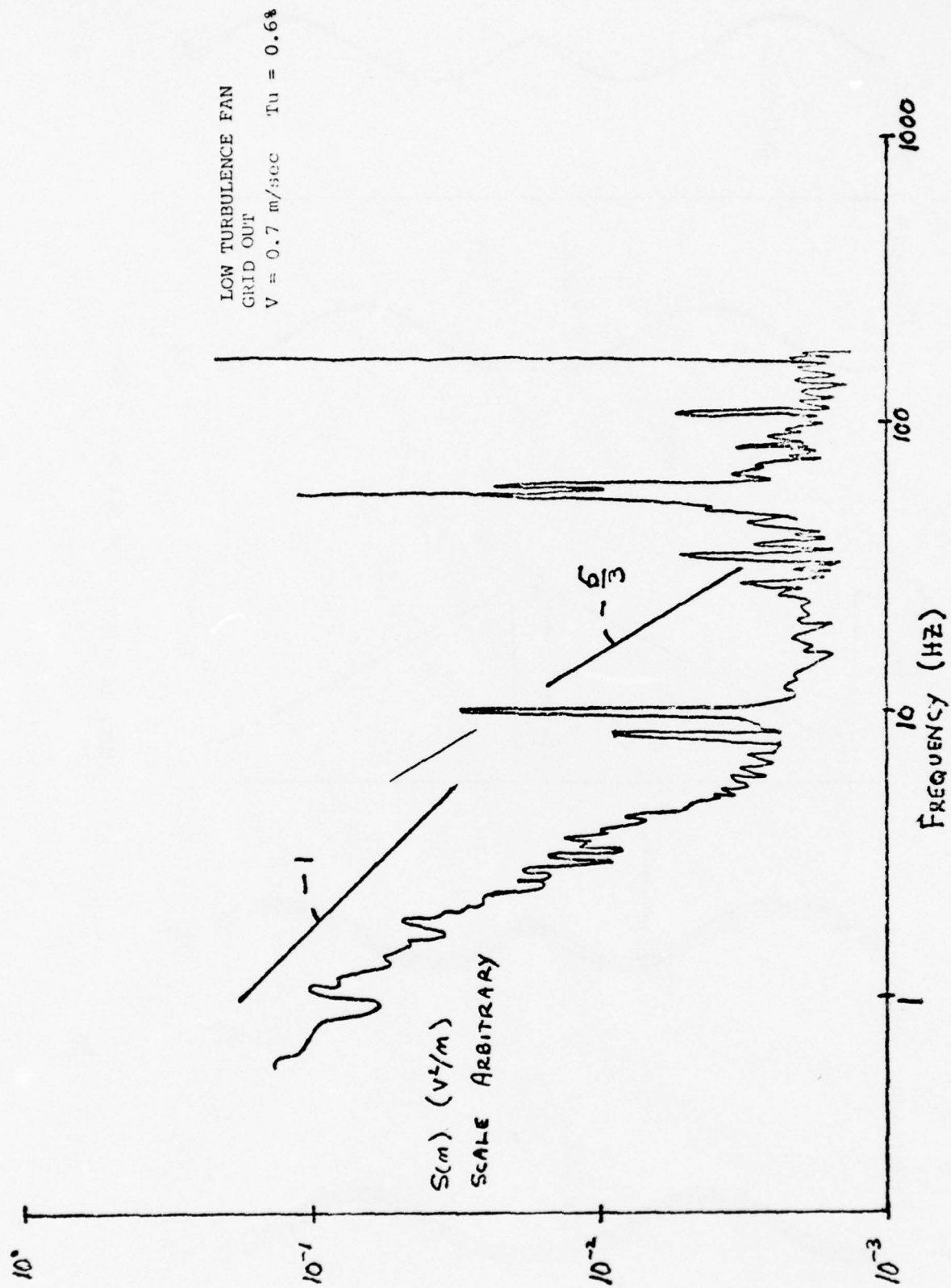
FIG. 17 COMPOSITE FREQUENCEY SPECTRUM FROM HOT WIRE - RUN 13

33

MAIN MOTOR
GRID OUT
V = 0.6 m/sec
Tu = 0.4%

FILTERED SIGNALS
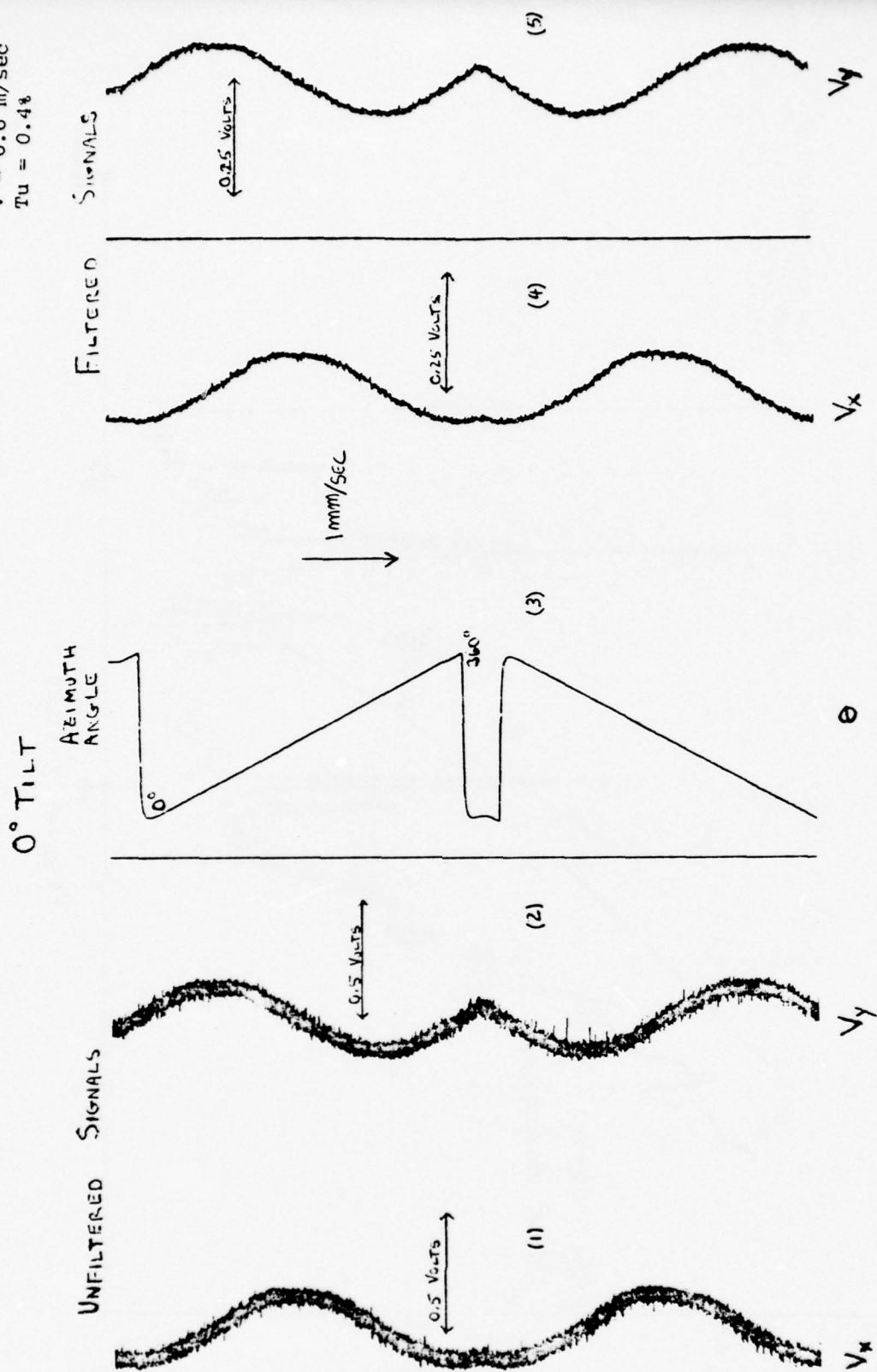
FIG. 18 CHART RECORDER DATA - RUN 20

34

MAIN MOTOR
GRID OUT
V = 3.2 m/sec
Tu = 0.8%

+30° TILT (LEADING EDGE UP)

SIGNALS

0.25 VOLTS

Peak behavior
Corona aligned
between posts

Valley occurs
when Corona
aligned behind
supporting posts

(5)

V_Y

FILTERED

0.25 VOLTS

(4)

V_X

$\frac{1\ mm}{sec}$

AZIMUTH ANGLE

30°

(3)

0°

Θ

SIGNALS

0.5 VOLTS

(2)

V_Y

UNFILTERED

0.5 VOLTS

(1)

V_X
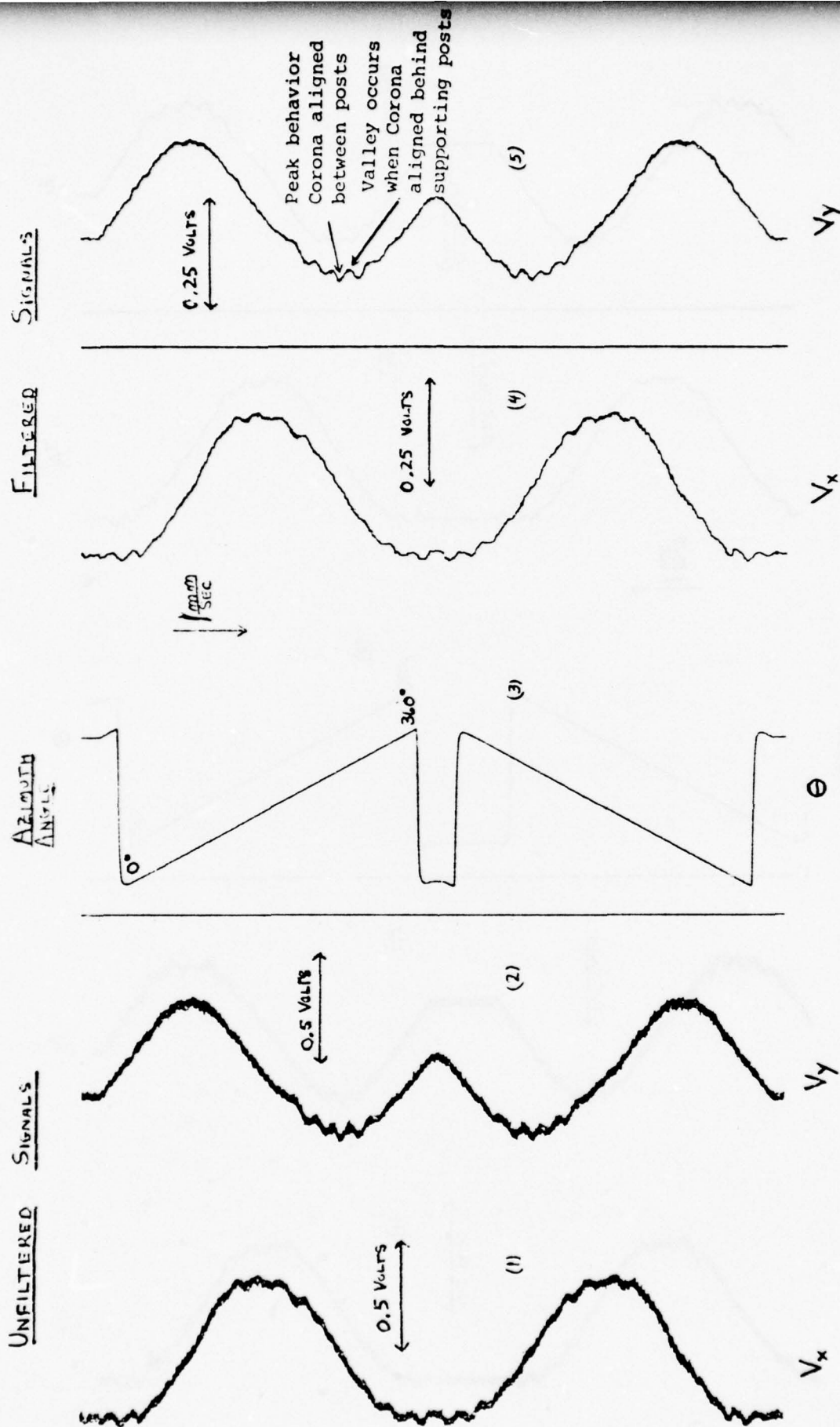
FIG. 19 CHART RECORDER DATA - RUN 28B

35

MAIN MOTOR
GRID OUT
V = 3.2 m/sec
Tu = 0.9%

-10° TILT (LEADING EDGE DOWN)

FILTERED SIGNALS

AZIMUTH ANGLE

UNFILTERED SIGNALS
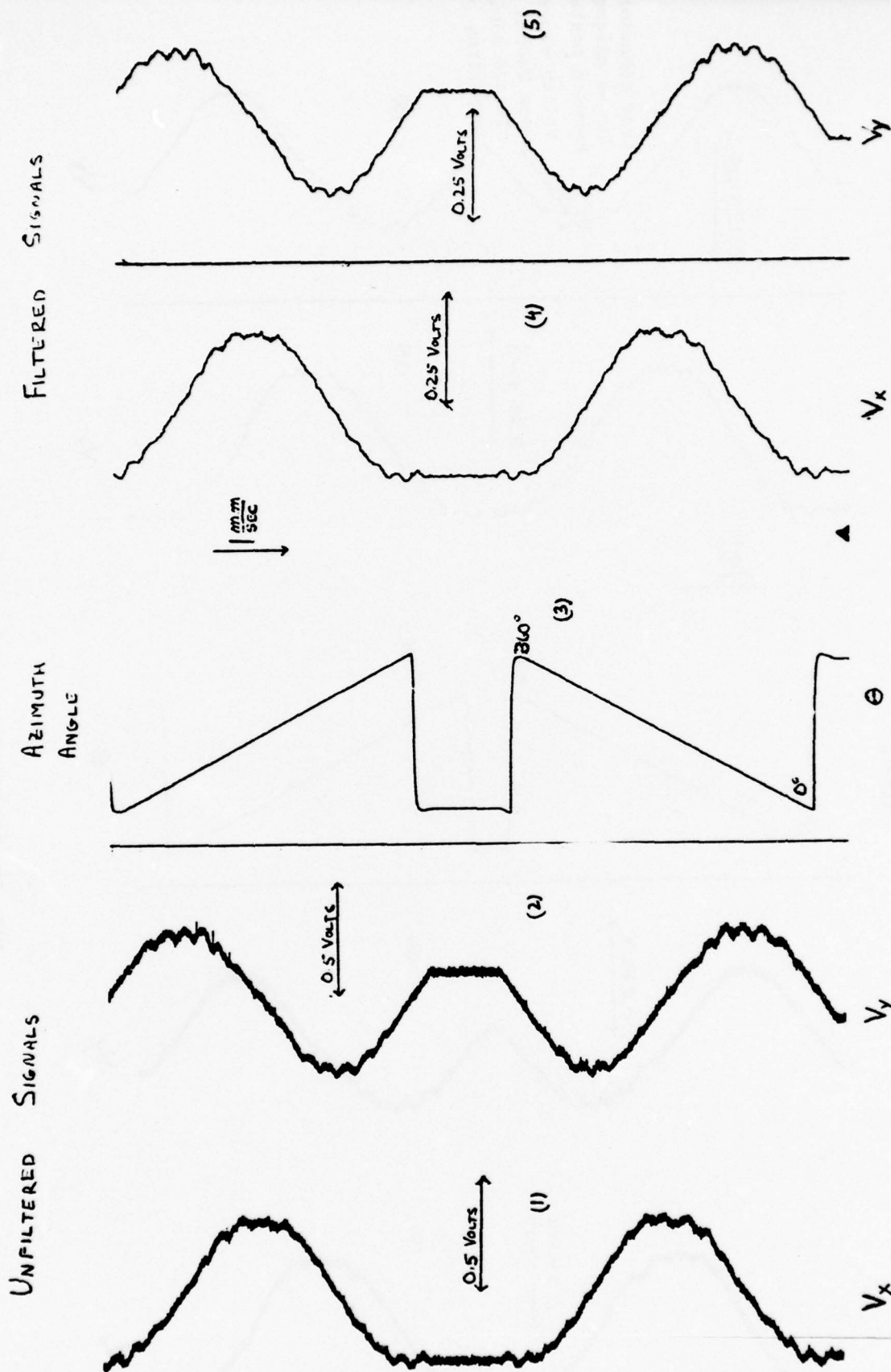
FIG. 20 CHART RECORDER DATA - RUN 28E

36
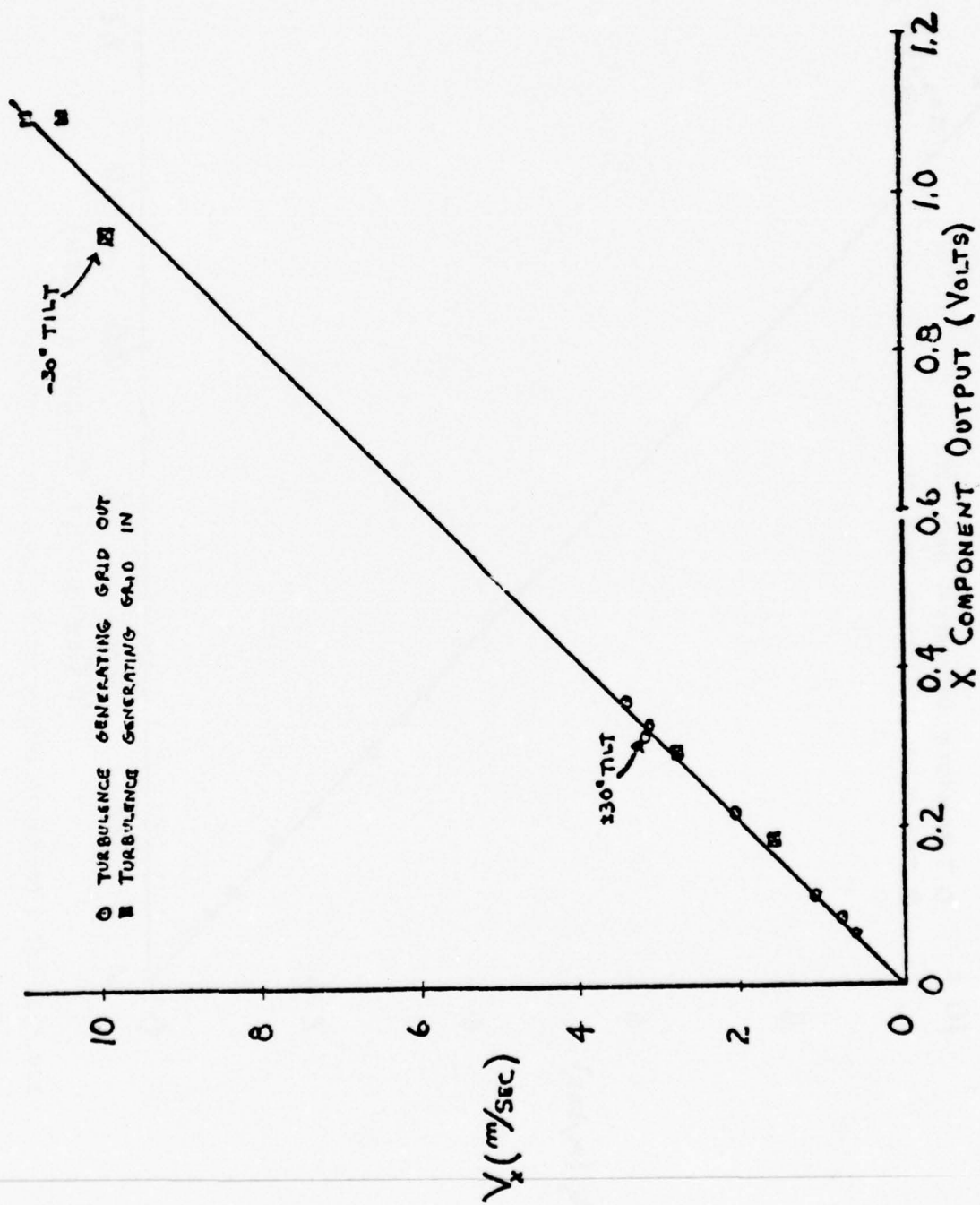
FIG. 21 TSI X COMPONENT OUTPUT VERSUS FREE STREAM VELOCITY
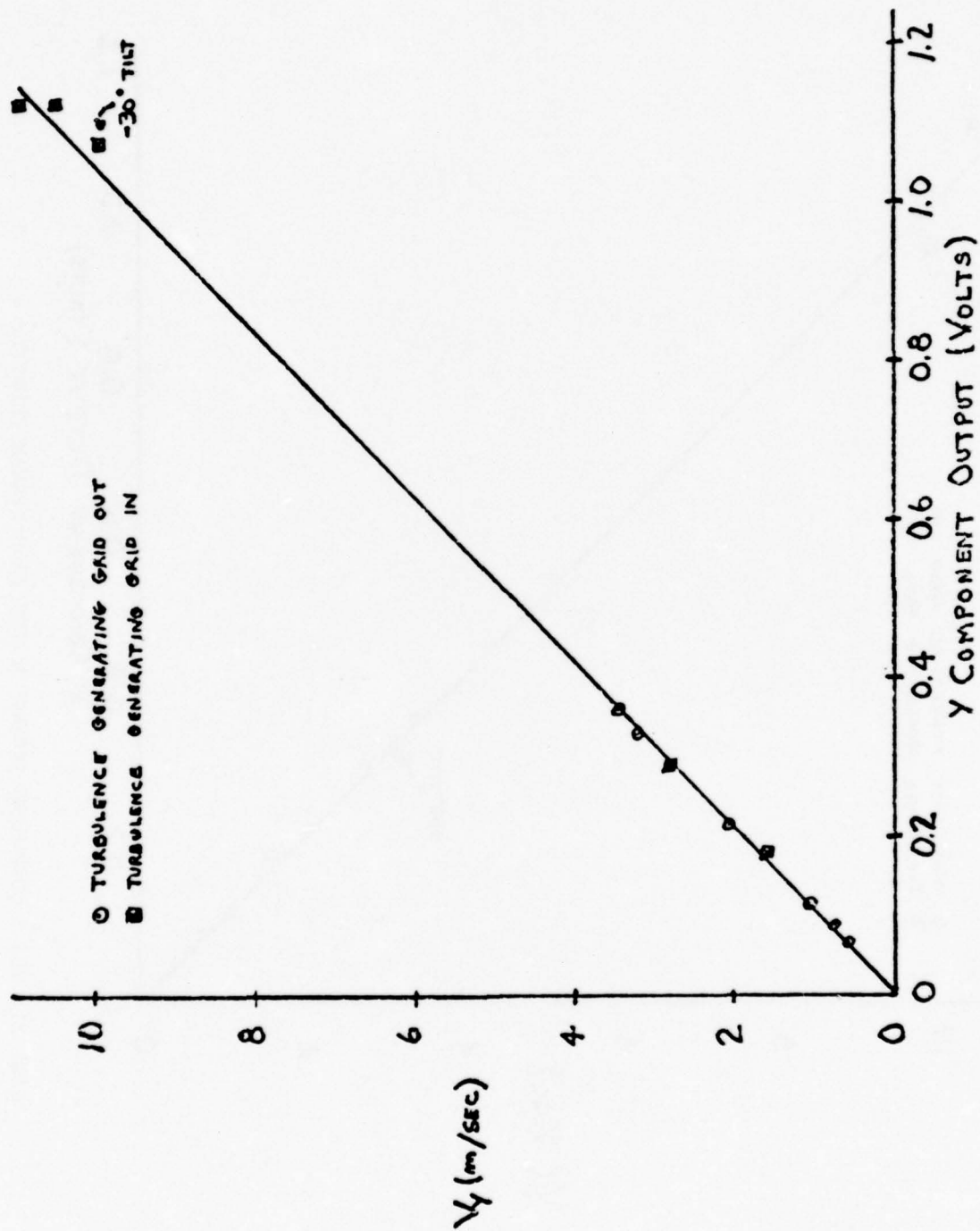
FIG. 22 TSI Y COMPONENT OUTPUT VERSUS FREE STREAM VELOCITY
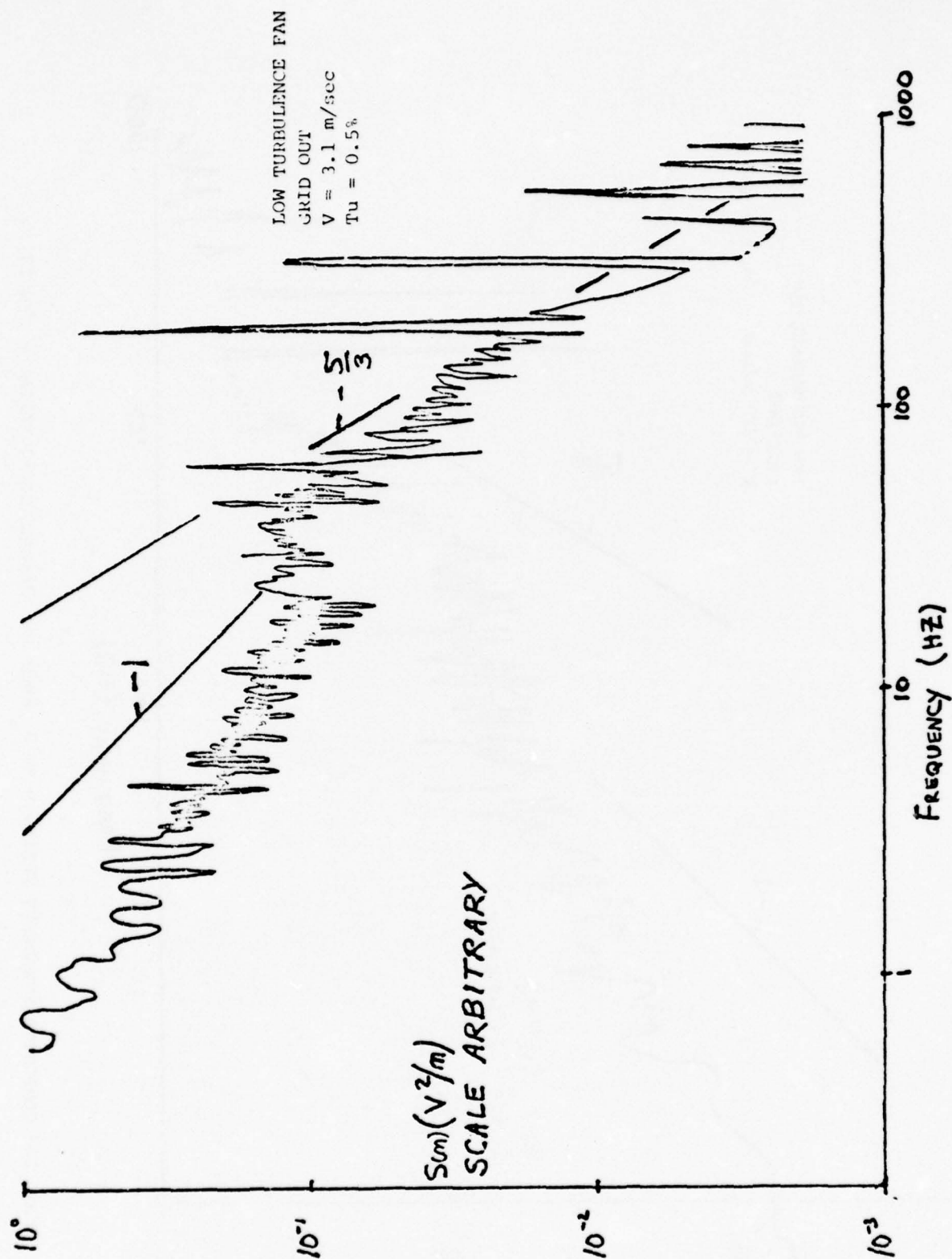
FIG. 23 COMPOSITE FREQUENCY SPECTRUM OF V_x FROM TSI ANEMOMETER AT PEAK – RUN 22

39

LOW TURBULENCE FAN
GRID OUT
V = 3.1 m/sec   Tu = 0.6%

$-\frac{5}{3}$

-1

S(m) (v^2/m)
SCALE ARBITRARY

10^1

10^{-1}

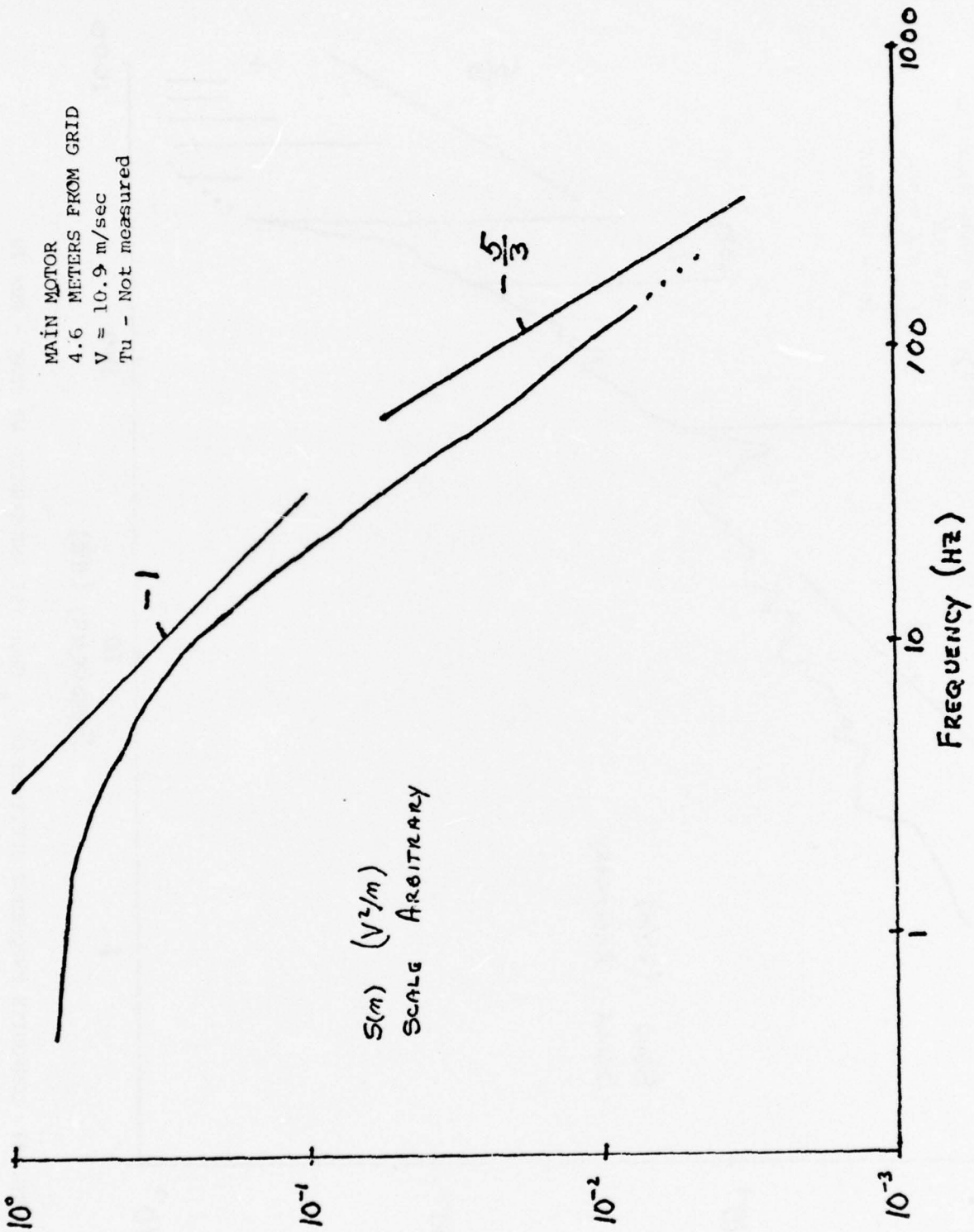10^{-2}

10^{-3}

1   10   100   1000
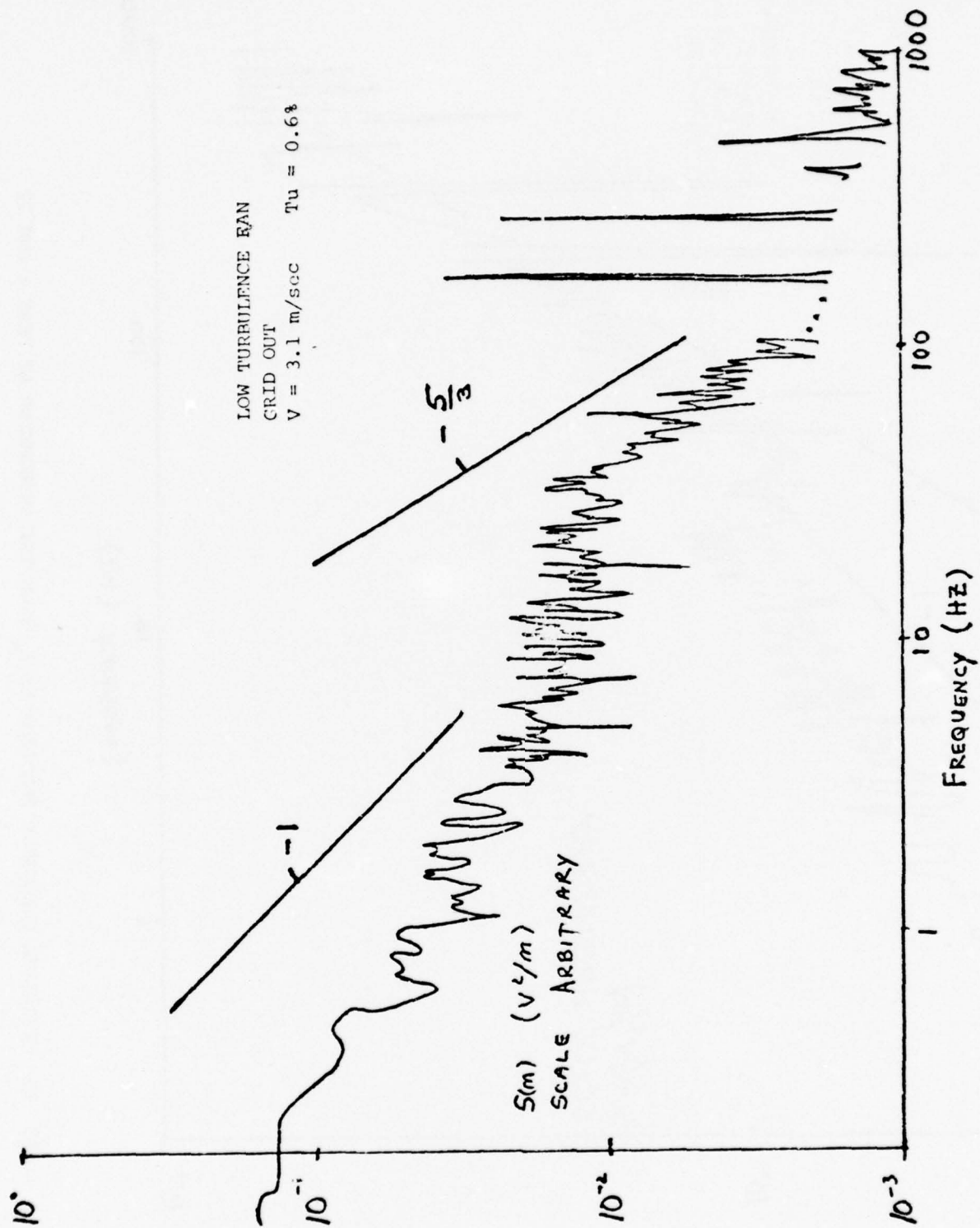
FREQUENCY (HZ)

FIG. 24 COMPOSITE FREQUENCY SPECTRUM OF V_x FROM TSI ANEMOMETER AT VALLEY - RUN 23
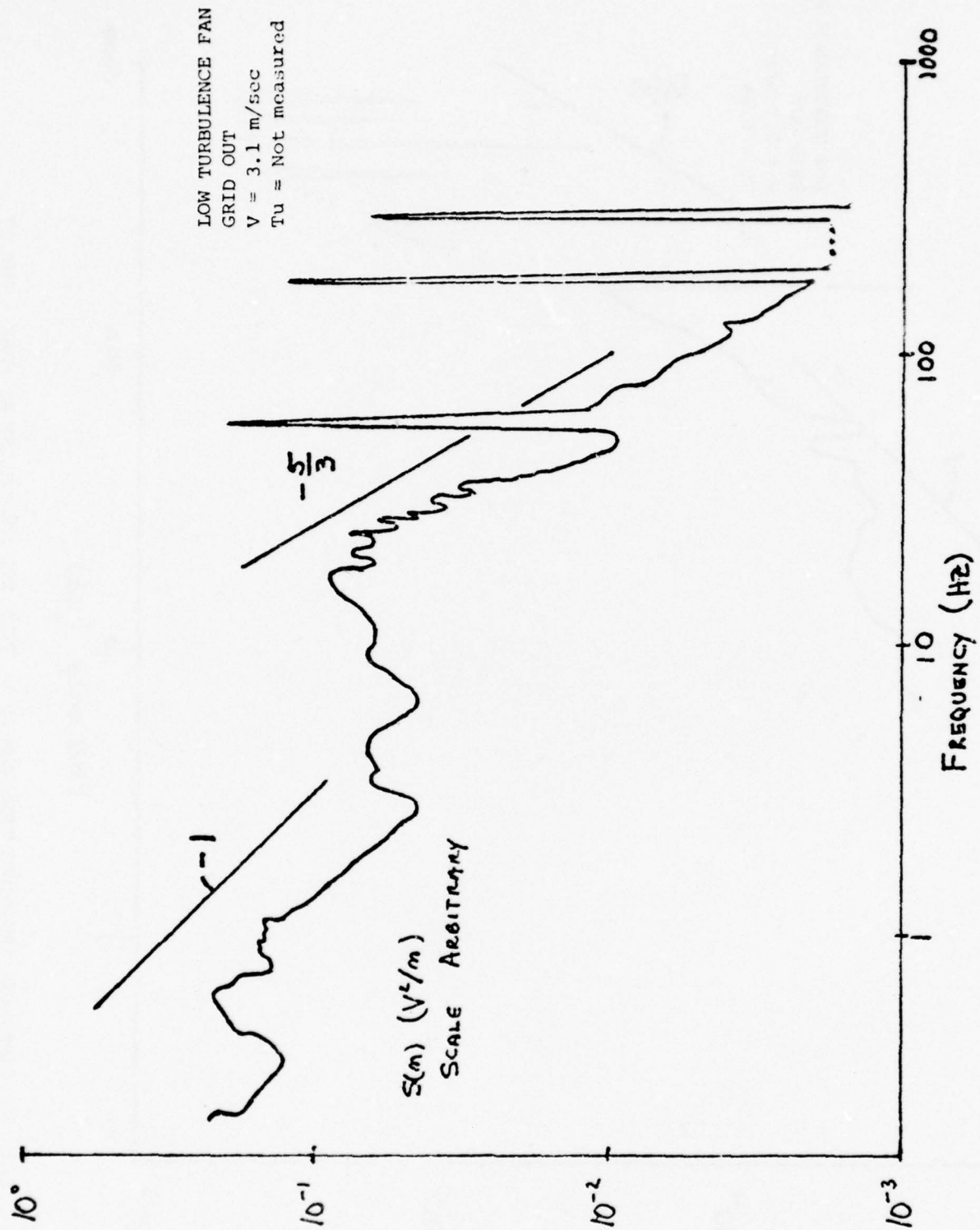
FIG. 25   COMPOSITE FREQUENCY SPECTRUM of V_x FROM TSI.   TSI COVERED – RUN 24
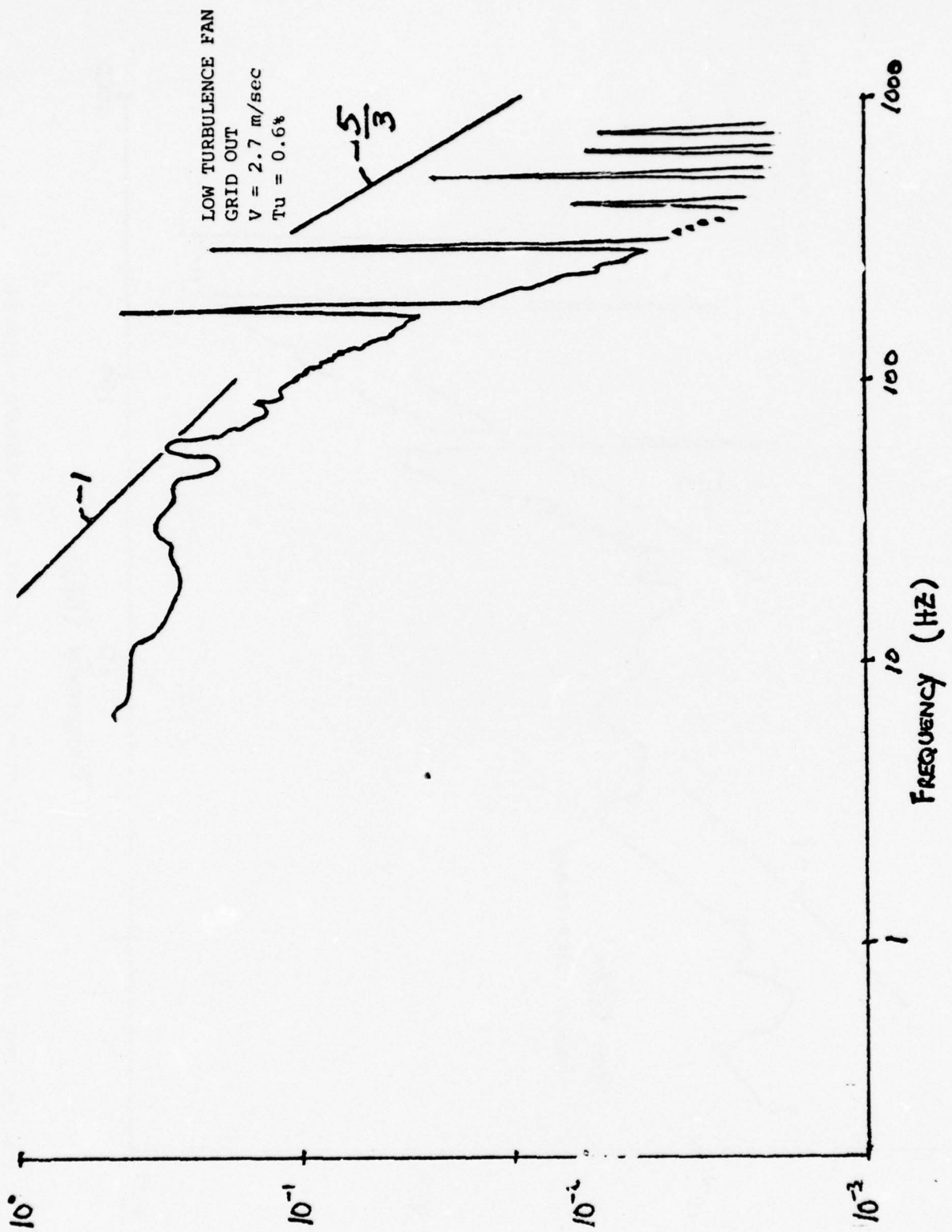
41

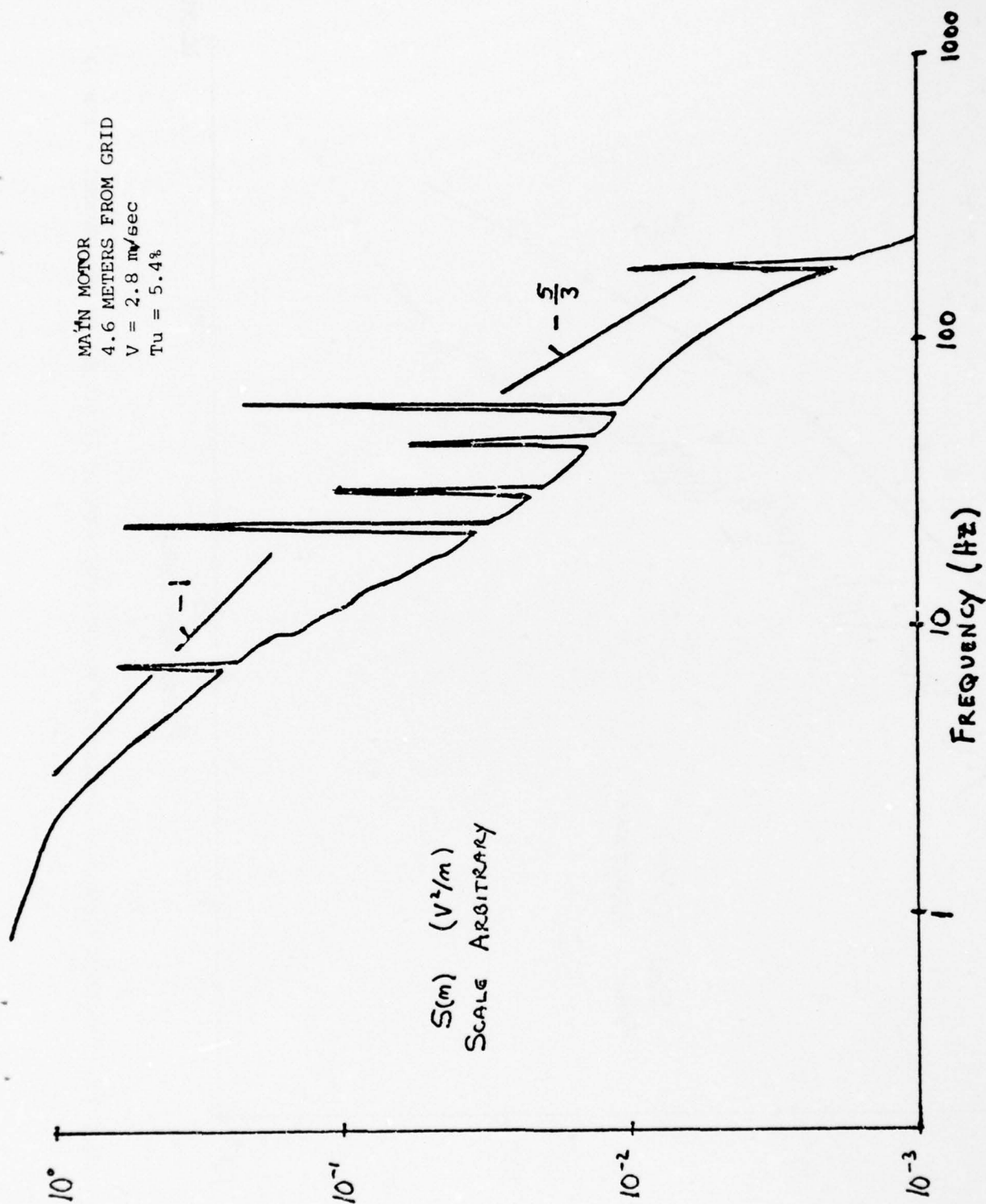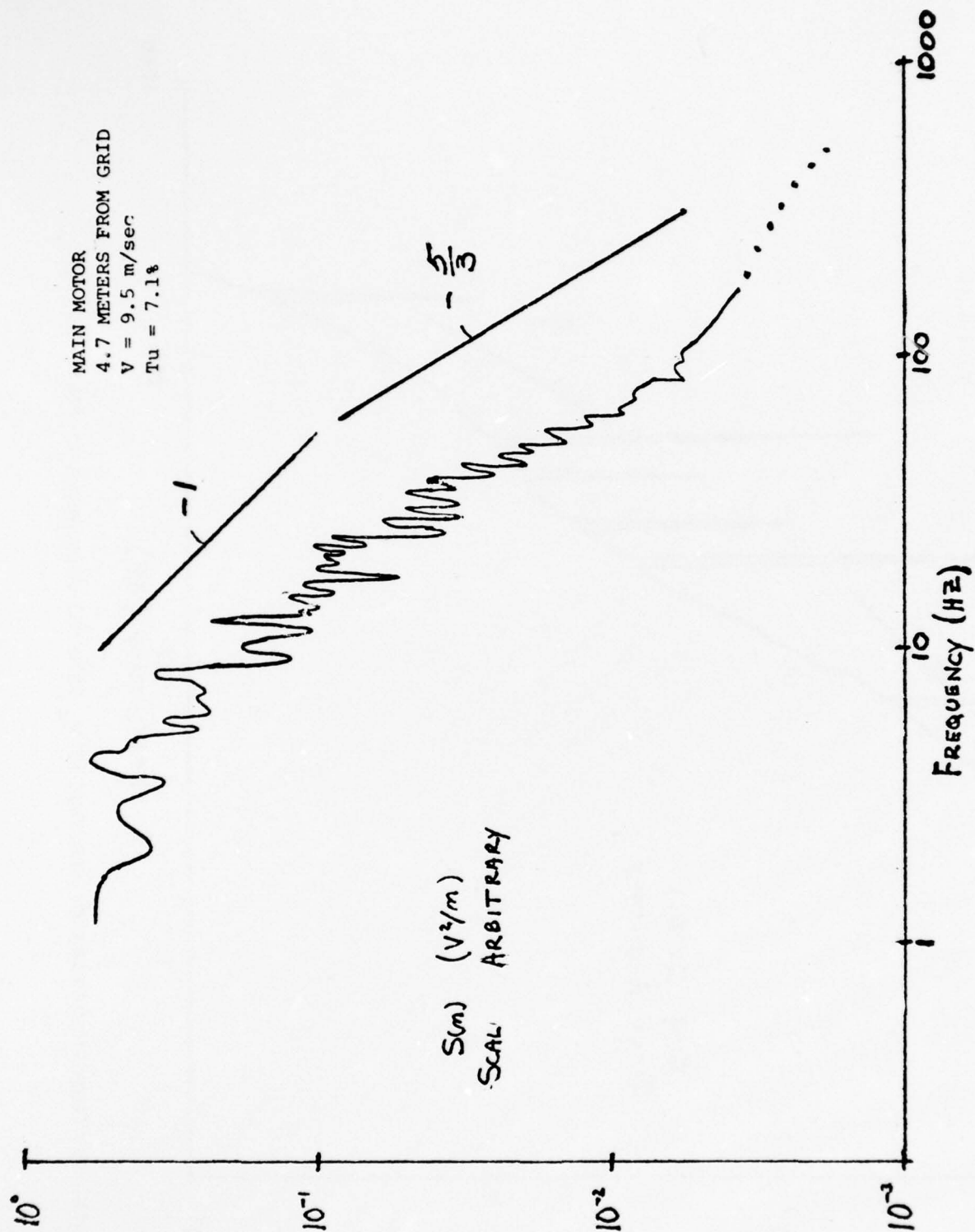FIG. 26   COMPOSITE FREQUENCY SPECTRUM OF V_x FROM TSI ANEMOMETER AT PEAK - RUN 27
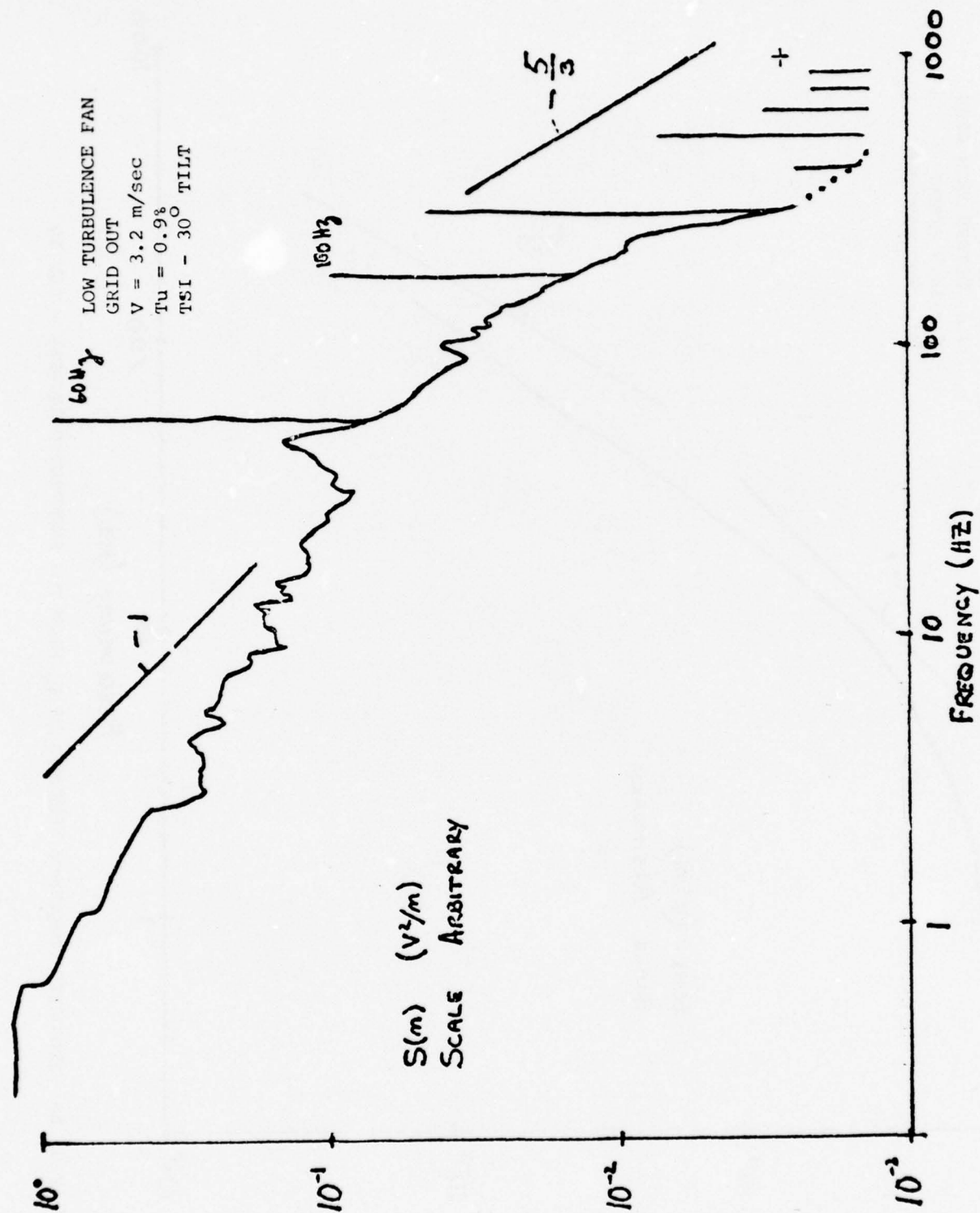
LOW TURBULENCE FAN
GRID OUT
V = 2.7 m/sec
Tu = 0.6%

$-\dfrac{5}{3}$

FREQUENCY (HZ)

42

FIG. 27 COMPOSITE FREQUENCY SPECTRUM OF V_x FROM TSI ANEMOMETER AT PEAK - RUN 29

43

MAIN MOTOR
4.6 METERS FROM GRID
V = 10.9 m/sec
Tu – Not measured

FIG. 28 COMPOSITE FREQUENCY SPECTRUM OF V_x FROM TSI ANEMOMETER AT PEAK – RUN 30

MAIN MOTOR
4.6 METERS FROM GRID
V = 2.8 m/sec
Tu = 5.4%

$-\frac{5}{3}$

-1

$S(m)$ (V^2/m)
SCALE ARBITRARY

FREQUENCY (Hz)

FIG. 29   COMPOSITE FREQUENCY SPECTRUM OF V_x FROM TSI ANEMOMETER AT PEAK - RUN 31

FIG. 30 COMPOSITE FREQUENCY SPECTRUM FROM HOT WIRE MOUNTED AT CENTER OF TSI CHANNEL - RUN 33

MAIN MOTOR
4.7 METERS FROM GRID
V = 9.5 m/sec
Tu = 7.1%

5/3

S(n) (V²/m)
SCALE ARBITRARY

FREQUENCY (Hz)

46

FIG. 31 COMPOSITE FREQUENCY SPECTRUM FROM HOT WIRE IN FREE STREAM - RUN 34

47

MAIN MOTOR
4.6 METERS FROM GRID
V = 3.7 m/sec
Tu = 5.1%
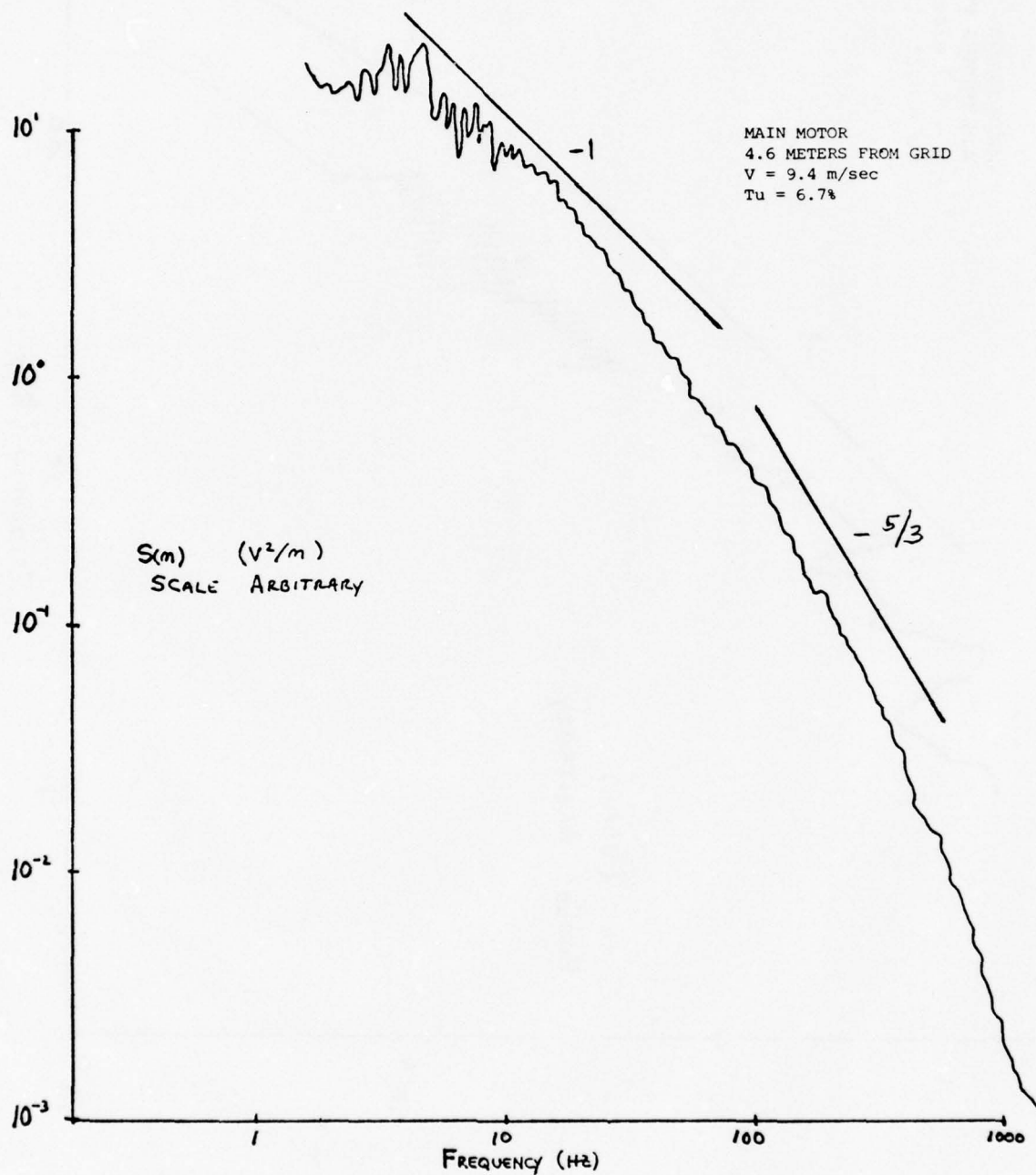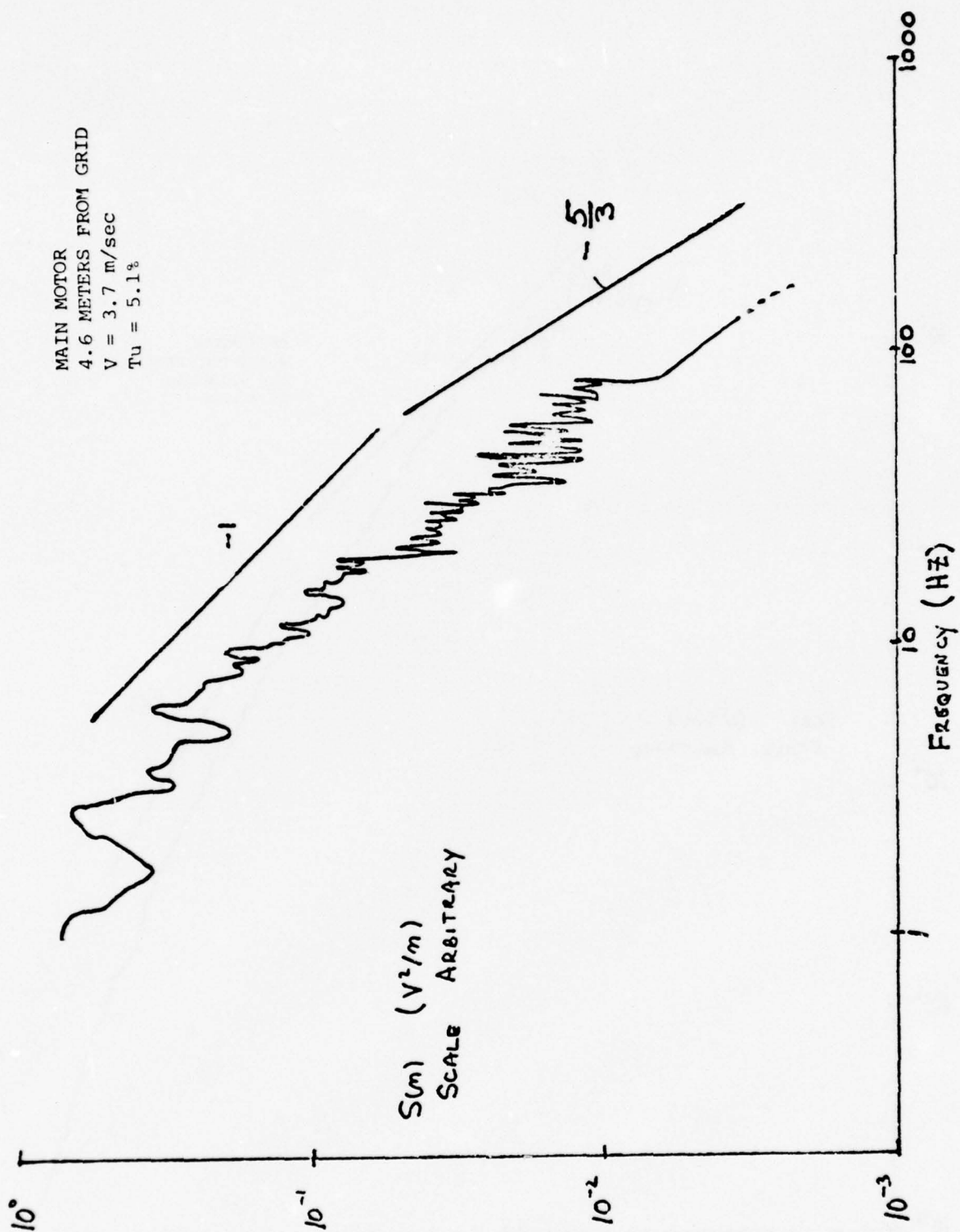
FIG. 32 COMPOSITE FREQUENCY SPECTRUM FROM HOT WIRE IN FREE STREAM – RUN 35

48
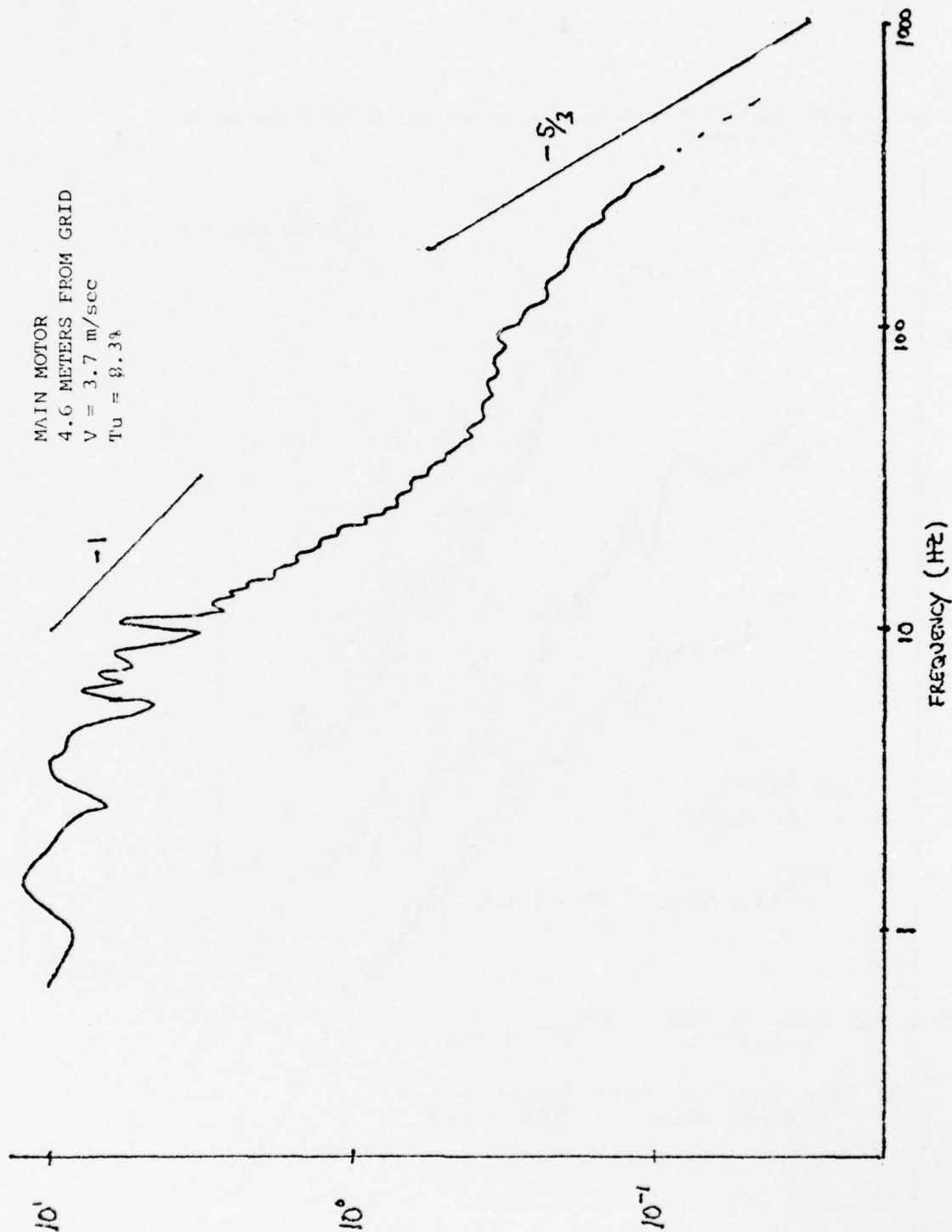
FIG. 33 COMPOSITE FREQUENCY SPECTRUM FROM HOT WIRE AT CENTER OF TSI - RUN 36

49

FIG. 34   COMPOSITE FREQUENCY SPECTRUM FROM TSI, AND HOT WIRE IN FREE STREAM AND AT
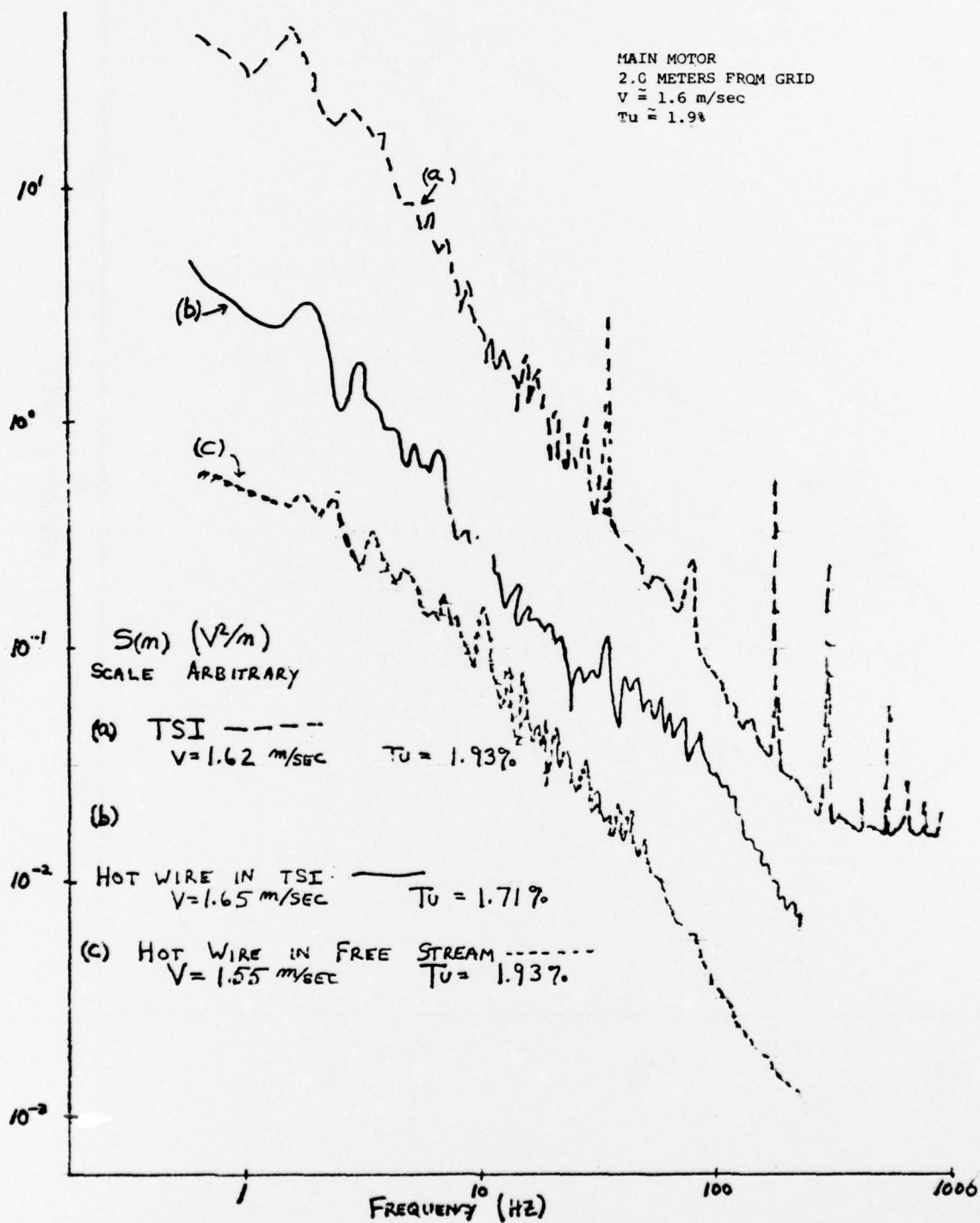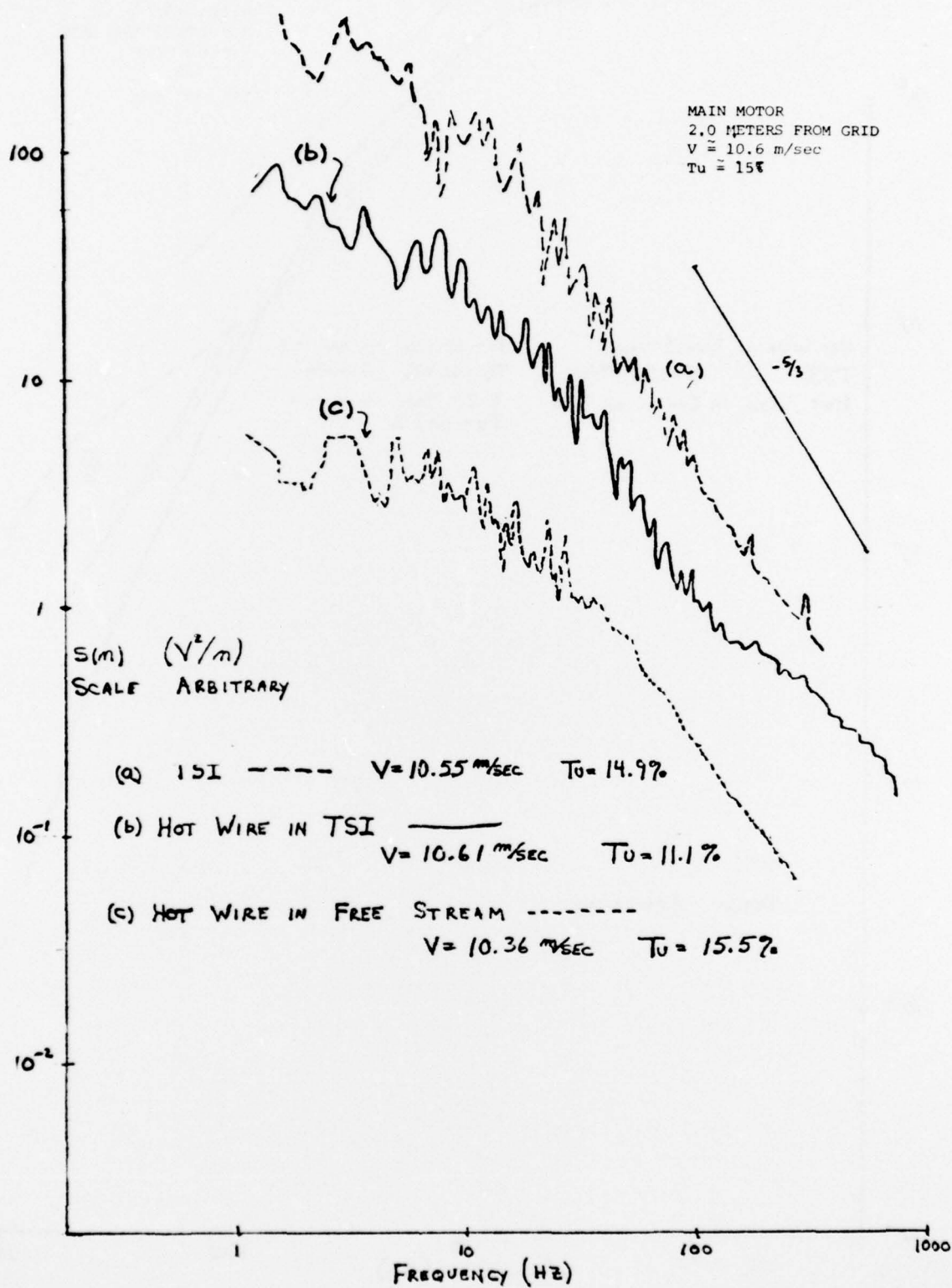   CENTER OF TSI - RUN 37


MAIN MOTOR
2.0 METERS FROM GRID
V ≅ 1.6 m/sec
Tu ≅ 1.9%

$S(m)$ (V^2/m)
SCALE ARBITRARY

(a) TSI ————
     V=1.62 m/sec   Tu = 1.93%

(b)

HOT WIRE IN TSI ————
     V=1.65 m/sec   Tu = 1.71%

(c) HOT WIRE IN FREE STREAM ———————
     V= 1.55 m/sec   Tu= 1.93%

FREQUENCY (HZ)

50

MAIN MOTOR
2.0 METERS FROM GRID
$V \cong 10.6$ m/sec
$Tu \cong 15\%$

100

(b)

-5/3

10

(a)

(c)

1

$S(n)$ (V^2/n)
SCALE ARBITRARY

(a) TSI ---- $V = 10.55$ m/sec $Tu = 14.9\%$

(b) HOT WIRE IN TSI ——
          $V = 10.61$ m/sec $Tu = 11.1\%$

10^{-1}

(c) HOT WIRE IN FREE STREAM --------
          $V = 10.36$ m/sec $Tu = 15.5\%$

10^{-2}

1   10   100   1000

FREQUENCY (HZ)

51

FIG. 36 COMPOSITE FREQUENCY SPECTRUM FROM TSI AND HOT WIRE IN FREE STREAM AND AT CENTER OF TSI - RUN 39
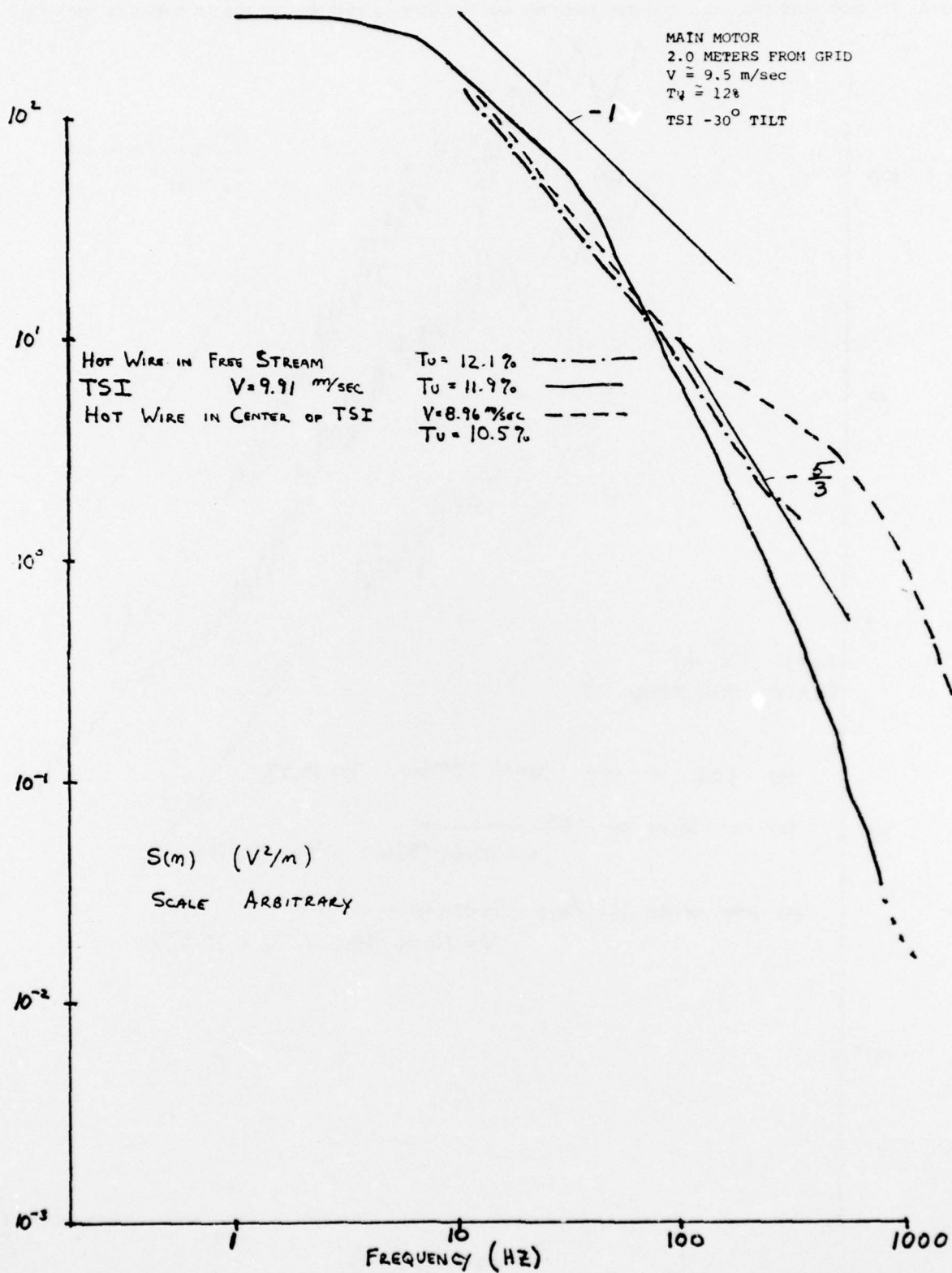
FIG. 37 COMPOSITE FREQUENCY SPECTRUM FROM TSI AND FROM HOT WIRE IN AND OUT OF TSI - RUN 40
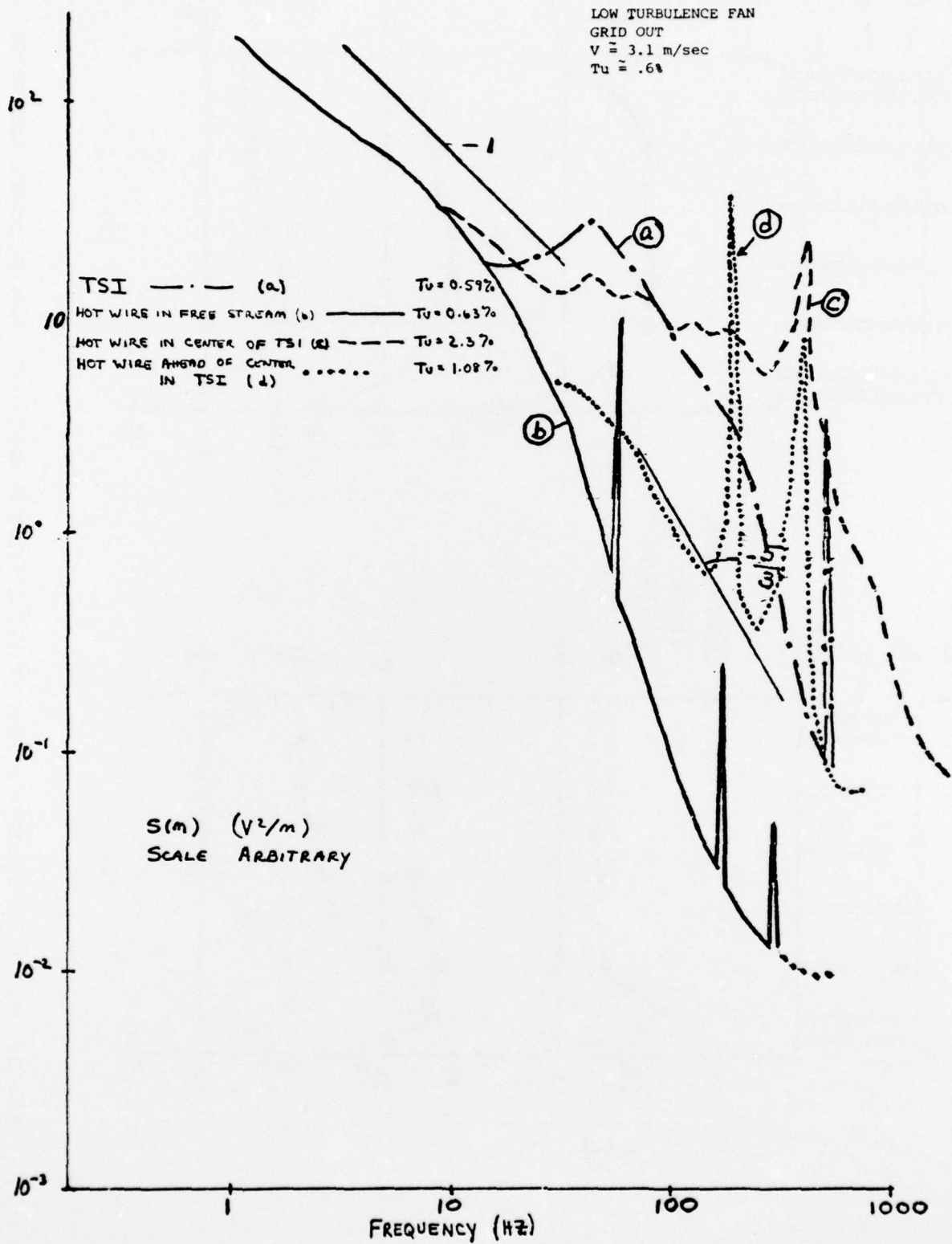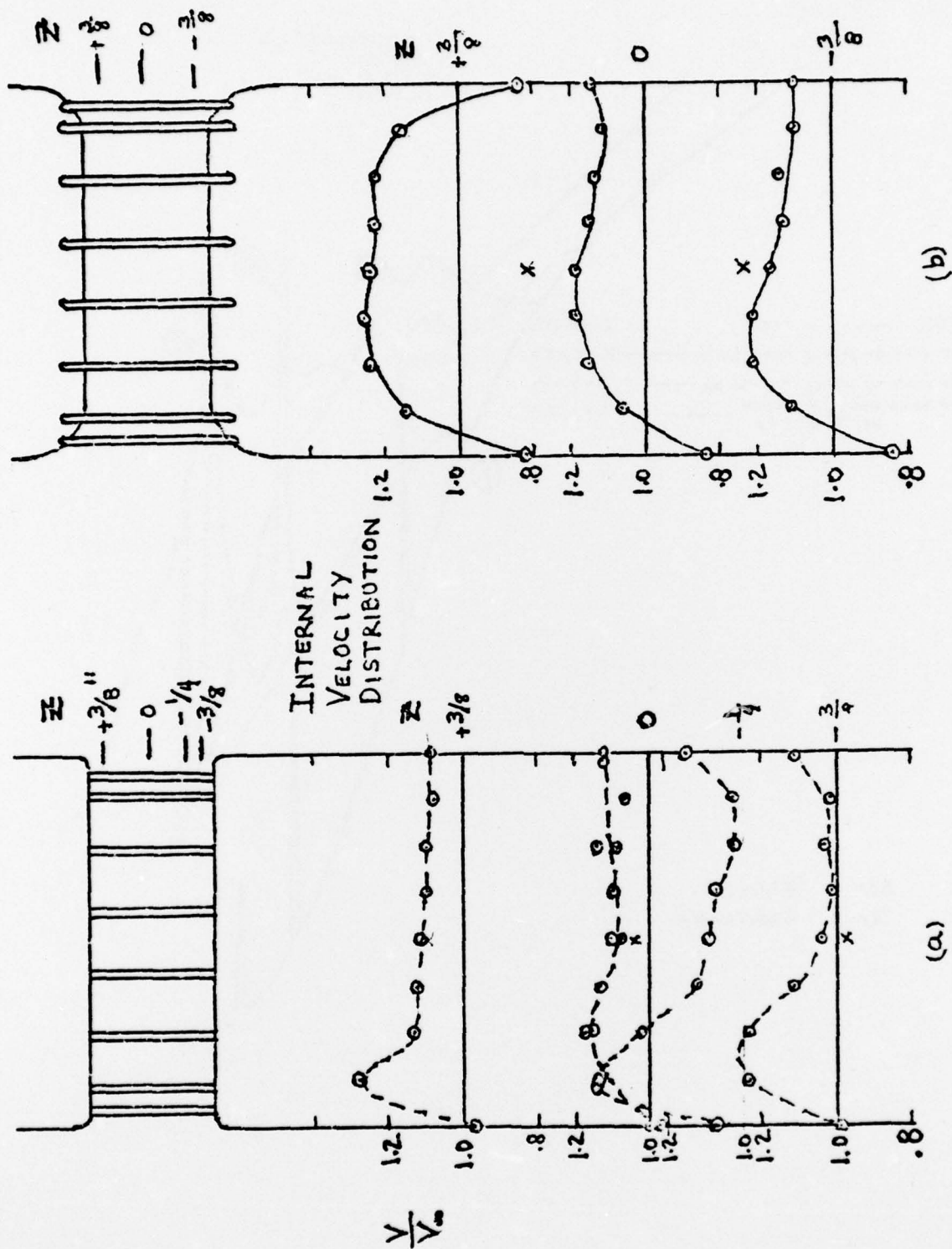
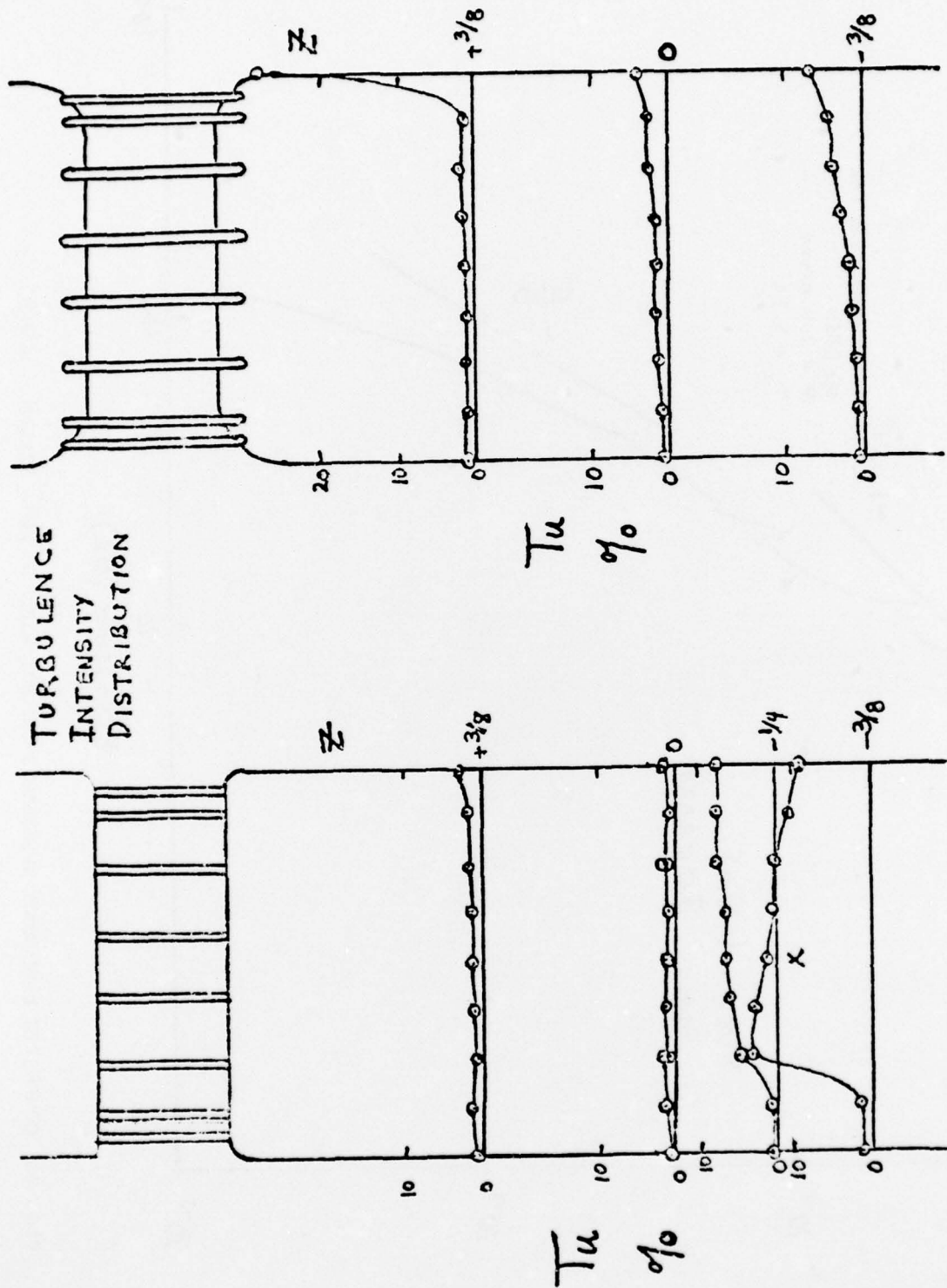FIG. 38 VELOCITY DISTRIBUTION INSIDE FIRST AND SECOND MODELS OF CORONA DISCHARGE ANEMOMETER

54

FIG. 39   TURBULENCE INTENSITY DISTRIBUTION INSIDE FIRST AND SECOND MODELS OF CORONA DISCHARGE
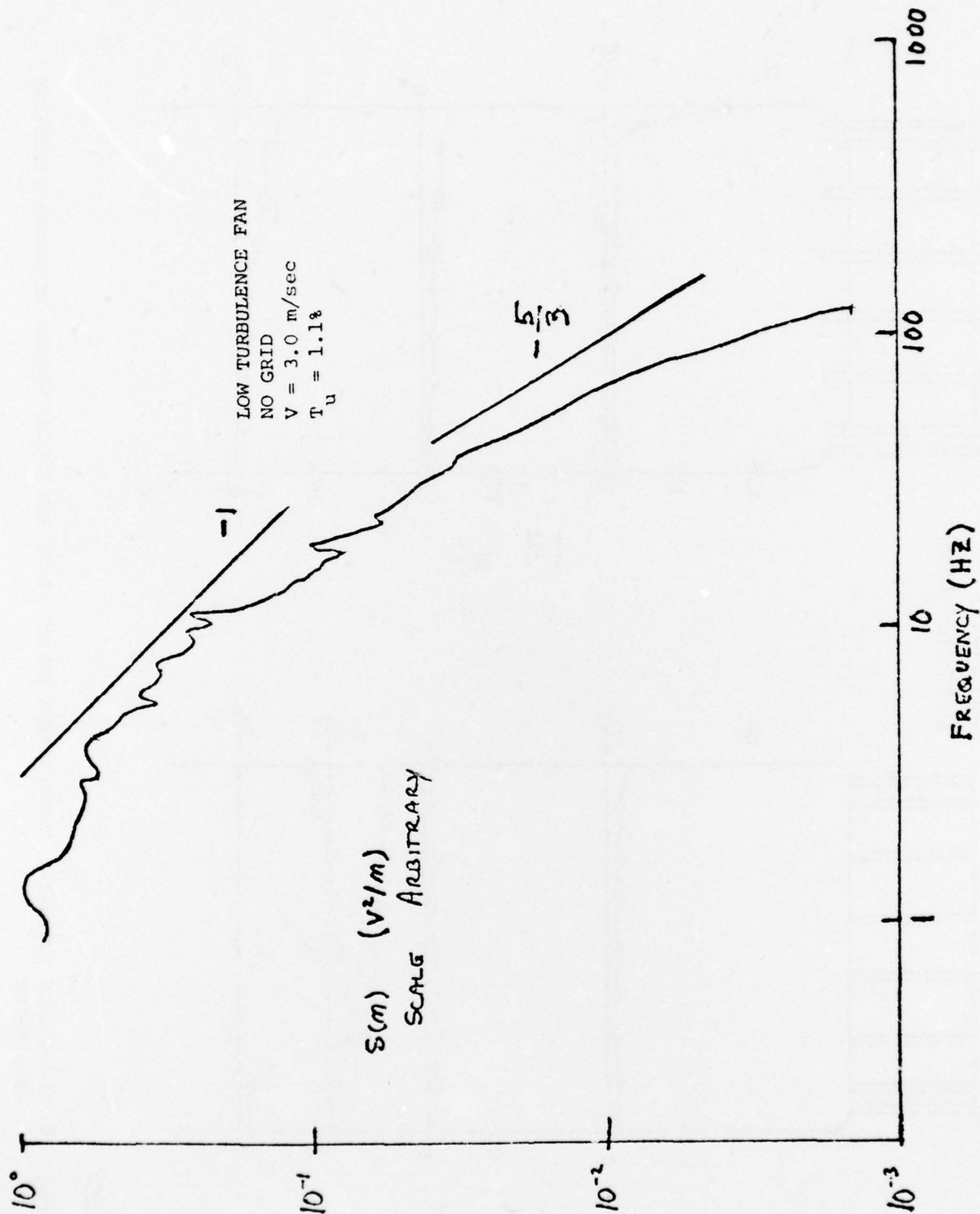ANEMOMETER

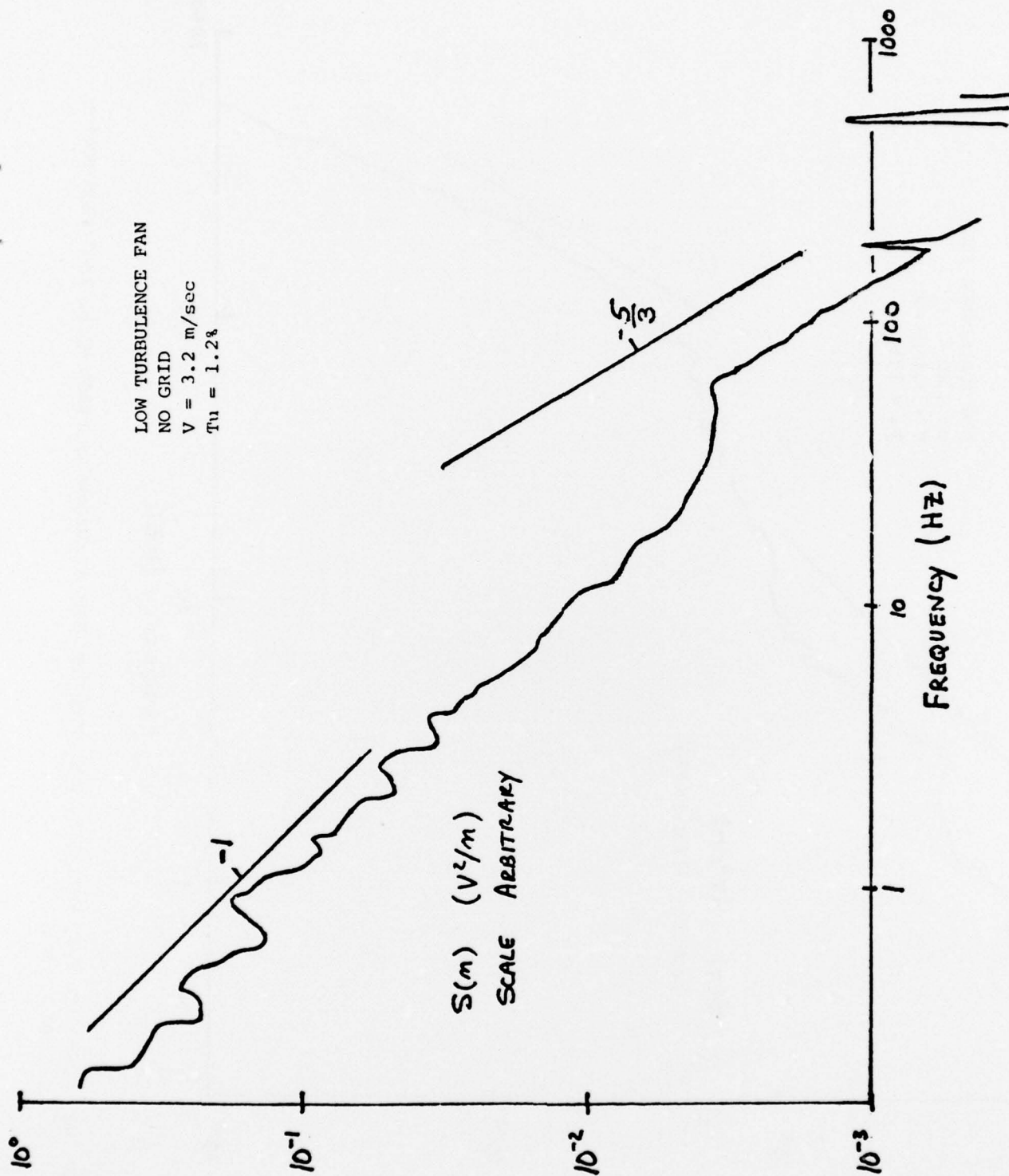FIG. 40 COMPOSITE FREQUENCY SPECTRUM FROM HOT WIRE IN FREE STREAM – RUN 50

56

LOW TURBULENCE FAN
NO GRID
V = 3.2 m/sec
Tu = 1.2%

FIG. 41 COMPOSITE FREQUENCY SPECTRUM FROM HOT WIRE AT CENTER OF FIRST CORONA DISCHARGE MODEL - RUN 51

57

LOW TURBULENCE FAN
NO GRID
V = 3.1 m/sec
Tu = 15%

$S(m)$ (V^2/m)
SCALE ARBITRARY

FREQUENCY (HZ)

$-\frac{5}{3}$

-1

10^0

10^{-1}

10^{-2}

10^{-3}
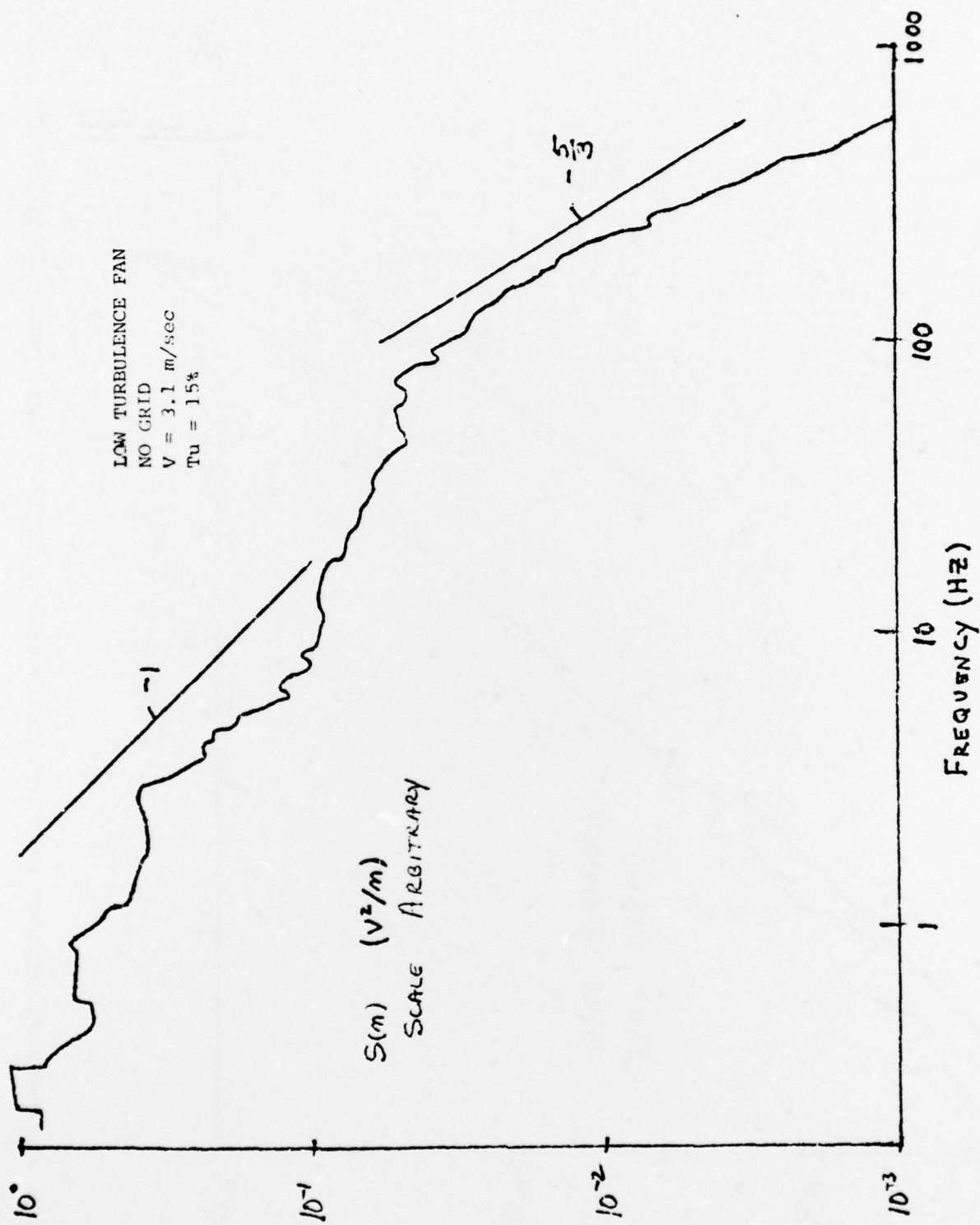
1

10

100

1000

FIG. 42   COMPOSITE FREQUENCY SPECTRUM FROM HOT WIRE AT CENTER OF FIRST MODEL 1/8" FROM BOTTOM
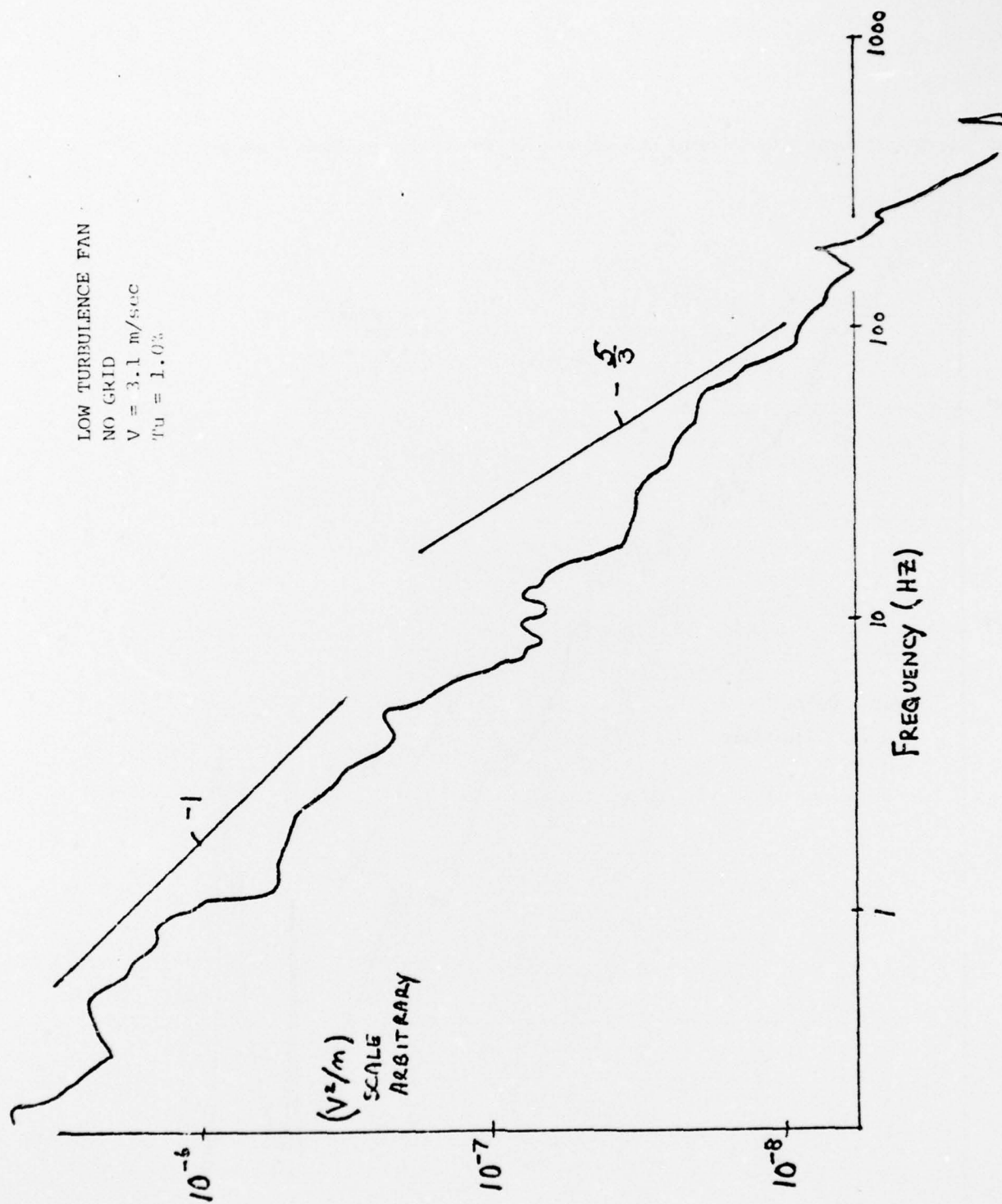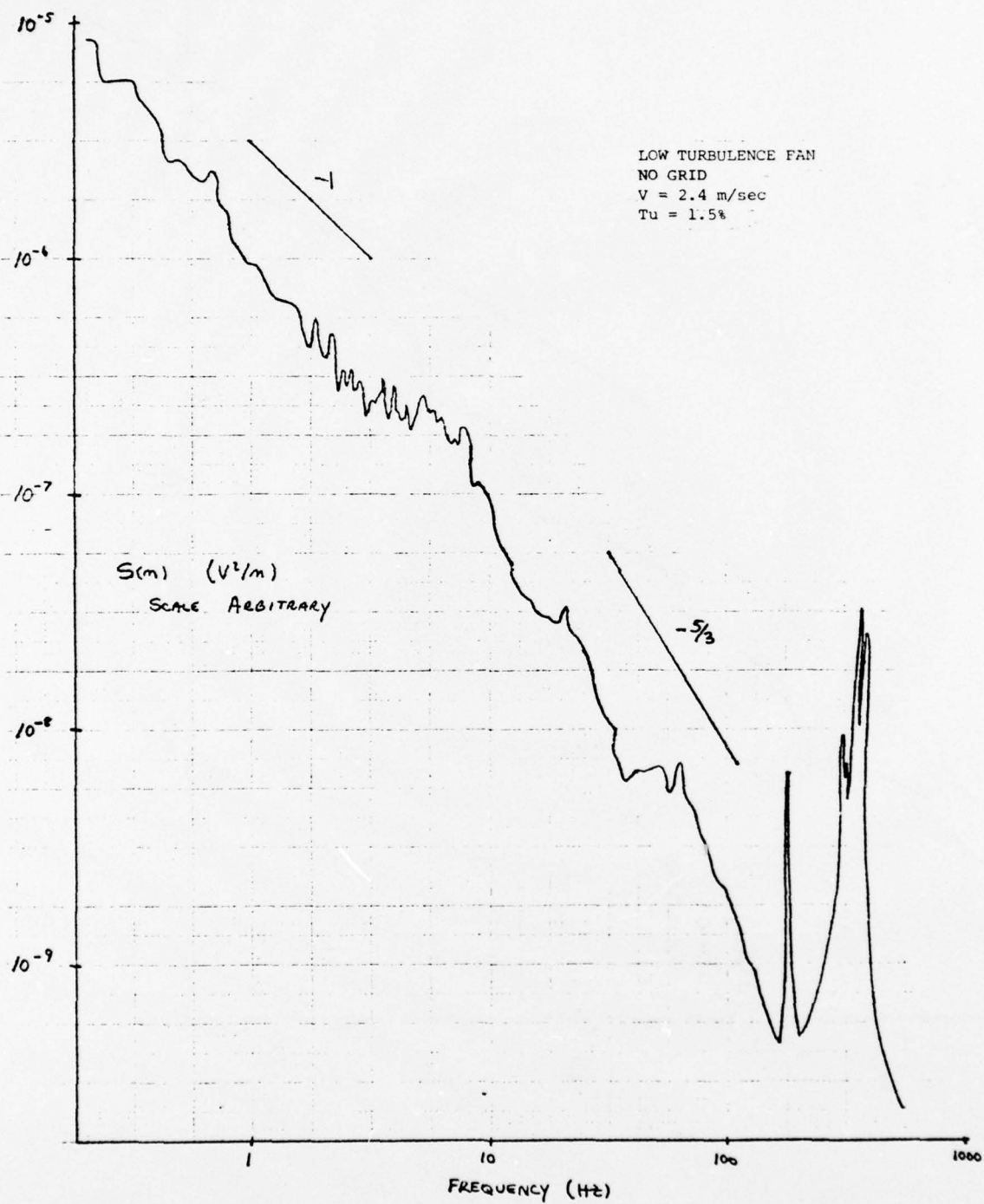CYLINDER - RUN 52

FIG. 43 COMPOSITE FREQUENCY SPECTRUM FROM HOT WIRE AT CENTER OF FIRST MODEL 1/16" FROM TOP CYLINDER – RUN 53

FIG. 44 COMPOSITE FREQUENCY SPECTRUM FROM HOT WIRE AT CENTER OF SECOND MODEL - RUN 57
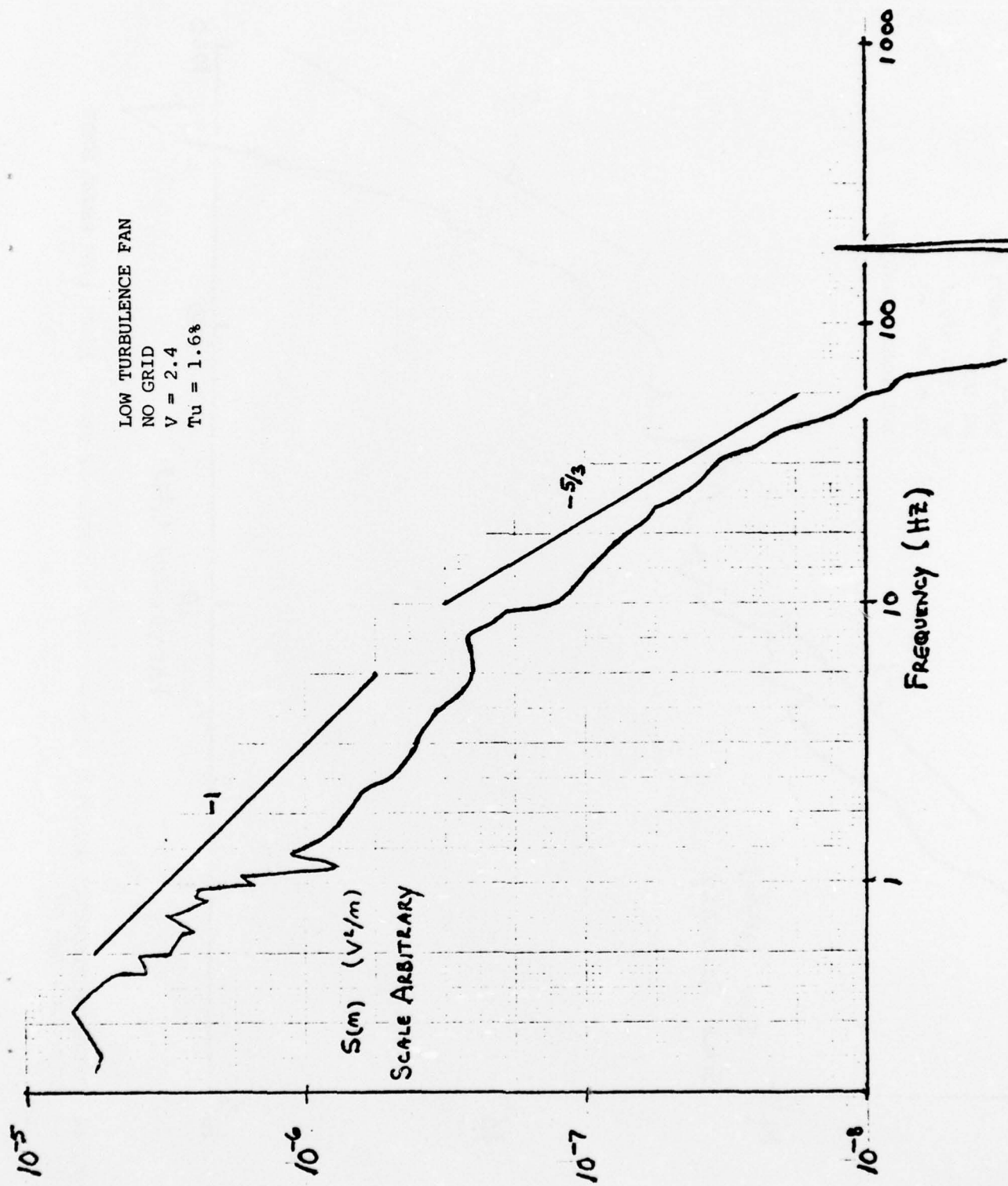

LOW TURBULENCE FAN
NO GRID
V = 2.4 m/sec
Tu = 1.5%

$S(m)$ (V^2/m)

SCALE ARBITRARY

-1

$-5/3$

FREQUENCY (Hz)

60

FIG. 45 COMPOSITE FREQUENCY SPECTRUM FROM HOT WIRE AT CENTER OF SECOND MODEL 1/8" BELOW CENTER
OF CYLINDER - RUN 60

61
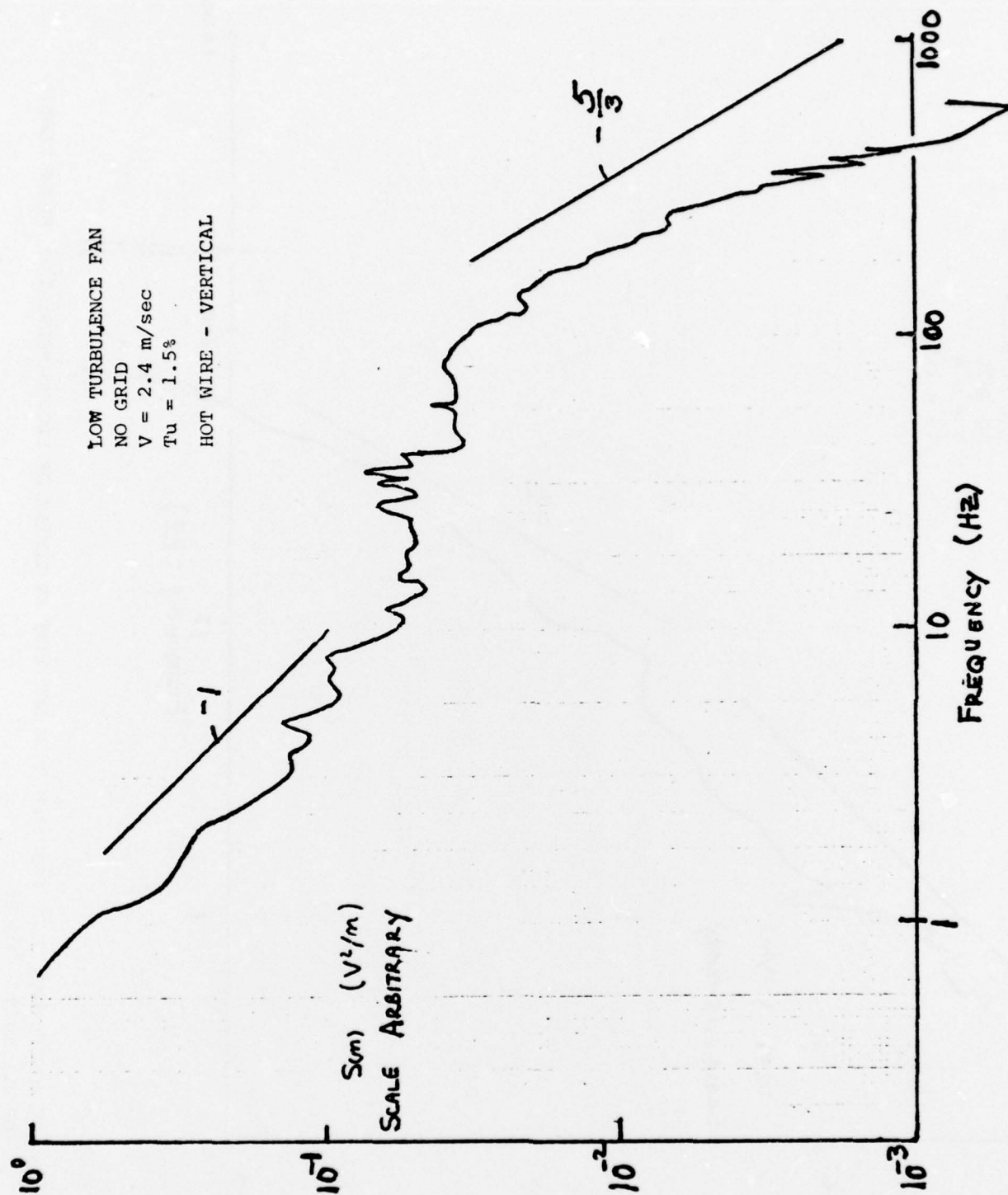
LOW TURBULENCE FAN
NO GRID
V = 2.4 m/sec
Tu = 1.5%

HOT WIRE - VERTICAL

FIG. 46 COMPOSITE FREQUENCY SPECTRUM FROM HOT WIRE AT CENTER OF SECOND MODEL 1/8" ABOVE LOWER
CYLINDER - RUN 59

62

LOW TURBULENCE FAN
GRID OUT
V = 2.4 m/sec
Tu = 1.5%

HOT WIRE - HORIZONTAL

5/3

-1

$S_{(n)}$ (V^2/m)
SCALE ARBITRARY

10^{-4}

10^{-5}

10^{-6}

10^{-7}

1

10
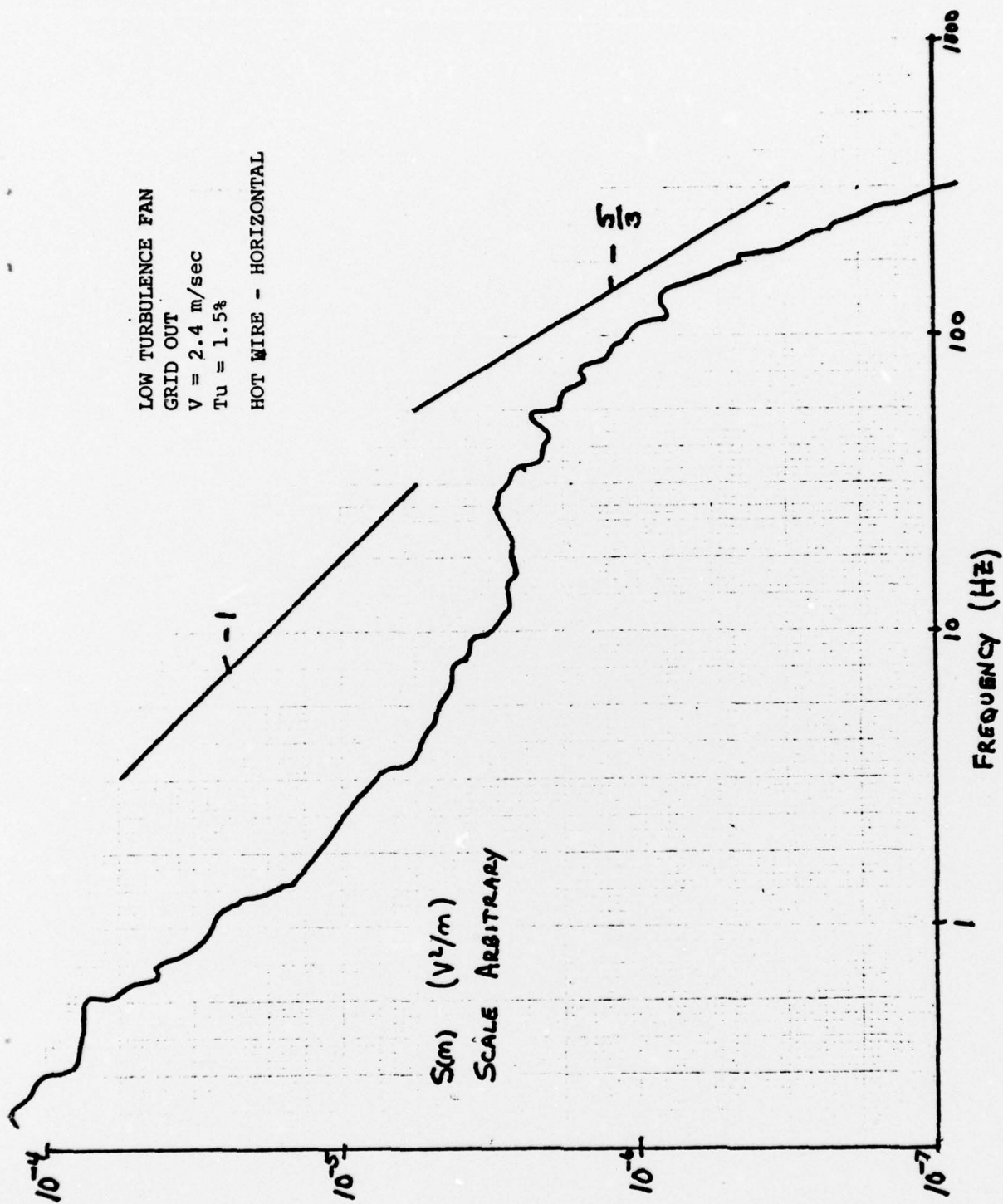
100

1000

FREQUENCY (Hz)

FIG. 47   COMPOSITE FREQUENCY SPECTRUM FROM HOT WIRE AT CENTER OF SECOND MODEL 1/8" ABOVE LOWER
CYLINDER - RUN 59

63